Final Report: Remote Sensing Based Assessment for Evaluating Risk to Transportation Infrastructure Following Wildfires

Richard Coffman, Thomas Oommen, Keith Weber

University of Arkansas, Michigan Technological University, Idaho State University
USDOT Cooperative Agreement No. OASRTRS-14-H-UARK

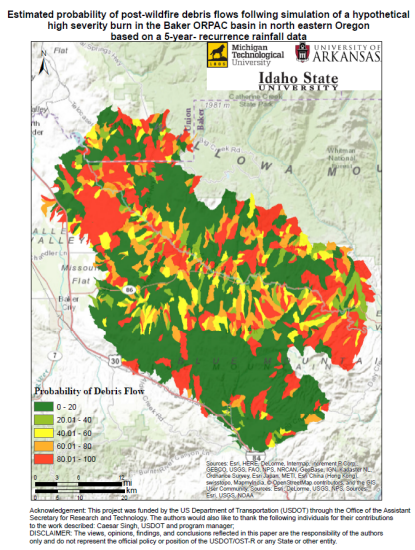

Principal Investigator: Richard Coffman, PhD, PE, PLS
Associate Professor
Department of Civil Engineering
University of Arkansas
4190 Bell Engineering Center
Fayetteville, AR 72701
(479) 575-8767
rick@uark.edu

Program Manager: Caesar Singh, PE
Director, University Grant Program
Office of the Assistant Secretary for Research and Technology (OST-R)
United States Department of Transportation
1200 New Jersey Avenue, E33-306
Washington, DC 20590
(202) 366-3252
caesar.singh@dot.gov

Table of Contents

Executive Summary 1
Chapter 1: Literature Review 2
1.1. Soil Parameters 2
1.2. Debris Flow Probability Models 3
1.3. Remote Sensing Instrumentation 4
Chapter 2: Development of Debris Flow Model 10
Chapter 3: Refinement of Debris Flow Model 11
3.1. Overview of the Decision Tree Methodology 12
3.2. Submitted Article of the Decision Tree Methodology 16
Chapter 4: Radar Remote Determination of Soil Properties 17
Chapter 5: Optical Remote Determination of Soil Properties 18
5.1. Abstract 18
5.2. Introduction 18
5.3. Review of Existing Methods 19
5.4. Materials and Methods 20
5.5. Results 26
5.6. Recommendations and Conclusions 35
Chapter 6: Development of a Ground-Based Remote Sensor 36
6.1. Instrument Design 38
6.2. Testing and Validation 41
Chapter 7: Conclusions, Outcomes, and Deliverables 43
7.1. Significant Findings and Outputs 44
7.2. Products and Outcomes 45
7.3. Post Project Initiatives 45
Chapter 8: References 47
Appendix A: Machine Learning Based Predictive Modeling
Appendix B: Assessment of Post-Wildfire Debris Flow
Appendix C: Volumetric Water Content Measurements
Appendix D: RECOVER Debris Flow Prediction Maps
Appendix E: Commercial Remote Sensing End User Workshop
Appendix F: SOTDiAL Patent Application

Executive Summary

The work and results obtained from the United States Department of Transportation (USDOT) Cooperative Agreement No. OASRTRS-14-H-UARK are presented within this final report. The objective of this project was to develop a remote sensing based decision support system for assessing the post-wildfire rockfall and mudslide hazards to roadways. The project was successful. A debris flow decision support system was developed and this system was integrated as a tool within the National Aeronautics and Space Administration (NASA) Rehabilitation Capability Convergence for Ecosystem Recovery (RECOVER) decision support system. Using this platform, post-wildfire debris flow models were requested from, and developed for, end users such as: NASA, the California Department of Transportation (CalTRANS), the Utah and Idaho Department of Lands (UDL and IDL, respectively), the Nevada, Idaho and Oregon State Offices of the Bureau of Land Management (BLM), and the National Oceanic and Atmospheric Administration (NOAA). The results of the project have been disseminated, through various workshops and presentations, to the following agencies: the Federal Highway Administration (FHWA), the United States Geological Survey (USGS), the Geological Surveys from the states of California, Oregon, Washington and Arizona, the Department of the Interior (DOI), the United States Forest Service (USFS), Idaho National Laboratory, CalTRANS, and the Departments of Transportation from the states of Colorado, Montana, and Utah.

This final report is divided into eight chapters. A review of the literature, as related to 1) soil parameters, 2) debris flow models for decision support systems for wildland fire applications, and 3) instrumentation to collect data for determination of debris flow risk is presented in Chapter 1. Information regarding the development and refinement of a debris flow model are contained in Chapter 2 (and Appendix A) and Chapter 3 (and in Appendix B). Discussion regarding the use of remote sensing, for the remote determination of soil properties, is described in Chapter 4 (and in Appendix C) and in Chapter 5. Likewise, discussion about the development of a ground-based remote sensing device for determination of post-fire debris flow susceptibility is provided in Chapter 6. Conclusions, outcomes, and deliverables from the project are presented in Chapter 7 and a comprehensive list of the references that were used in the document is included as Chapter 8. Developed debris flow probability models for the wildland fires, as requested by end users as a part of this project, are included as Appendix D. Likewise, for completeness, a summary of the end user workshop that was held at the conclusion of this project (on August 24, 2017) is provided in Appendix E. The summary of the workshop includes the information (Powerpoint slides) that was presented at the end user workshop. For completeness, the patent application that was filed for the Soil Observation Topographic Differential Absorption Lidar (SOTDiAL) ground-bsed device that was developed for this project is included as Appendix F. Additional details regarding the project, that is described herein, can be found on the project website: https://wildfire-landslide-risk-dss.uark.edu.

DISCLAIMER: The views, opinions, findings and conclusions reflected in this publication are solely those of the authors and do not represent the official policy or position of the USDOT/OST-R, or any State or other entity. USDOT/OST-R does not endorse any third party products or services that may be included in this publication or associated materials.

Acknowledgement: This work is supported by the US Department of Transportation, through the Office of the Assistant Secretary for Research and Technology (USDOT-OST-R). Additional information regarding this project can be found at https://wildfire-landslide-risk-dss.uark.edu.

Chapter 1: Literature Review

The literature review, which is provided in this chapter, is divided into three main parts. The three parts are comprised of the following: 1) soil parameters (Section 1.1), 2) debris flow models for decision support systems for wildland fire applications (Section 1.2), and 3) instrumentation to collect data for determination of debris flow risk (Section 1.3). The works that were cited in the literature review are listed in Section 1.4.

1.1. Soil Parameters

As early as 1960, Bishop et al. (1960) described the importance of understanding unsaturated soil properties for determination of the shear strength of soils. The understanding of unsaturated soil properties continues to receive scrutiny today. Soil water matric potential, also described as negative pore water pressure, or soil suction, is of particular concern to geotechnical engineers, because it often controls the effective stress within the soil deposit, thereby controlling the behavior of the soil. Soil suction is of particular interest in the context of slope stability. Slope failures have been attributed to the dissipation of near-surface soil suction and the resulting reduction in shear strength (Brackley et al. 1971, Lumb 1975, Fredlund 1981, Ho et al. 1982, Krahn et al. 1989, Blatz et al. 2004).

The unsaturated, near-surface slope failure mechanism, common to non-fire affected areas, is also frequently observed in the form of post-wildfire debris flows in fire affected areas. Each year, hundreds of wildfires in the United States, burn an average of 6,329,703 acres of land (10 year average, NIFC 2017). Many of these wildfires occur in mountainous areas, such as the Intermountain West and Southern California. Following the various fires, the denuded soil slopes are susceptible to debris flows, which may disrupt traffic, destroy homes, and threaten human life. Although these debris flows events have been difficult to predict, probabilistic modeling techniques continue to improve (Gartner et al. 2008, Cannon et al. 2010, Negri 2016, Kern et al. 2017). The understanding of unsaturated soil properties is critical to the prediction of these debris flows. To date, there is a lack of available soil property data. Furthermore, the small amount of data that are available are typically too dispersed to be useful in site-specific, predictive models, because the data were collected with low spatial or low temporal

resolution from airborne or spaceborne sensors, or from traditional in situ instrumentation.

1.2. Debris Flow Probability Models for Decision Support Systems

Mountainous regions in the western United States have been recognized for producing wildfire induced debris flows (Eaton 1936, Bailey et al. 1947, Wells 1987, Cannon and Degraff 2009). The majority of the debris flow material is believed to originate from channel erosion rather than hillside rill erosion (Santi et al. 2007). Erosional initiation processes may include progressive sediment entrainment during surface runoff process or failure of discrete slope slips after infiltration (Cannon et al. 2000). The ability to predict the probability of these post-wildfire debris flow events, regardless of initiation mechanisms, is essential to develop necessary precautions and to prevent infrastructure damage. The previous models developed to predict the probability of debris flow occurrence in the intermountain western United States were based on multivariate logistic regression and had 4-percent success rate of identifying debris flows (Cannon et al. 2010).

Advanced machine learning techniques, which use nonlinear variable relationships and interactions, have been applied with great success for probabilistic modeling in many environmental fields such as hydrological forecasting, satellite data processing, and ecological modeling (Benediktsson et al. 1990, Olden and Jackson 2002, Krasnopolsky 2007, Sahoo et al. 2007, Haupt et al. 2009, Hsieh 2009, Samui et al. 2012). Advanced modeling is particularly beneficial when assessing abundant remote sensing data describing information on air, land, and water, which permits methodical monitoring of the environment (Hsieh 2009). Without thoroughly understanding variable relationships, as well as debris flow processes, the large amounts of data collected may best be used with advanced statistical modeling techniques. As documented herein, nonlinear relationships from post-wildfire debris flow data, partially gathered remotely, were used to develop new models in prediction of probability of debris flows in burned basins through the use of advanced machine learning methods. The previous logistic regression models developed assumed a linear relationship between the log odds of p and the covariates (Cannon et al. 2010, Kuhn and Johnson 2013).

Advancements in satellite imagery and remote sensing allow for the generation of a larger amount of information much more rapidly than previous field assessments (NASA 2011, De Graff 2014). Prior to the use of satellite imagery, Burned Area Emergency Response (BAER) teams conduct field operations to develop soil burn severity maps, identify debris flow hazard, and assess debris flow risk where a hazard was identified. (De Graff and Lewis 1989). Recently, as according to Clark (2013), satellite imagery has been being used to determine a burned area reflectance classification (BARC), which is based on a transformation of the imagery into the differenced Normalized Burn Ratio (dNBR). Digital maps, created from the satellite imagery, are then incorporated into Geographic Information Systems (GIS) where soil and topographical information on studied basins is also available. This newer system is much more precise and consistent than previous field assessment methods and also allows more prompt response time (De Graff 2014). The aforementioned advancements in data

availability has led to developments in computer science and statistics and given rise to modern methods of classification and prediction, based on computer intensive techniques using data splitting and cross-validation, rather than statistical significance testing to identify, calibrate, and validate predictive schemes (Freedman 1983, Steyerberg and Harrell 2015).

A standard approach to building a predictive model is to randomly select a portion of the data for new model development and to use the remaining independent holdout data set for model validation. Various measures of accuracy are then used to evaluate the model's performance. To generate nearly unbiased predictions, while balancing variance, resampling techniques are used to estimate model efficacy during training of candidate models in order to represent better out-of-sample predictions (Kuhn and Johnson 2013). For these reasons, advanced modeling techniques are more rigorous and, therefore, preferred over more traditional statistical approaches.

1.3. Instrumentation used to Collect Data for Determination of Debris Flow Risk

Remote sensing of soil properties has been performed by utilizing a variety of sensors and techniques that operate within the electromagnetic spectrum (Figure 1.1). Techniques have included: passive imaging spectroscopy (multispectral, hyperspectral, Visible Near-Infrared [VNIR], Mid-Infrared [MIR], and Short-Wave Infrared [SWIR]), active and passive microwave systems (Synthetic Aperture Radar [SAR], Real Aperture Radar [RAR], Ground-Penetrating Radar [GPR]), and gamma-ray spectrometry (Wulf et al. 2015). A type of imaging spectroscopy called Diffuse Reflectance Infrared Fourier Transform (DRIFT) has been utilized to correlate reflectance spectra with a variety of soil properties, including water content (Park 1980, Dalal and Henry 1986, Ben-Dor and Banin 1995, Janik et al. 1995, Islam et al. 2003, Whiting et al. 2004, Tian and Philpot 2015, Philpot and Tian 2016, Garner 2017), sand content (Janik et al. 1995, Chang et al. 2001, Islam et al. 2003), silt content (Janik et al. 1995, Chang et al. 2001, Shepherd and Walsh 2002, Cozzolino and Moron 2003, Islam et al. 2003), and clay content (Janik and Skjemstad 1995, Ben-Dor and Banin 1995, Janik et al. 1995, Chang et al. 2001, Walvoort and McBratney 2001,

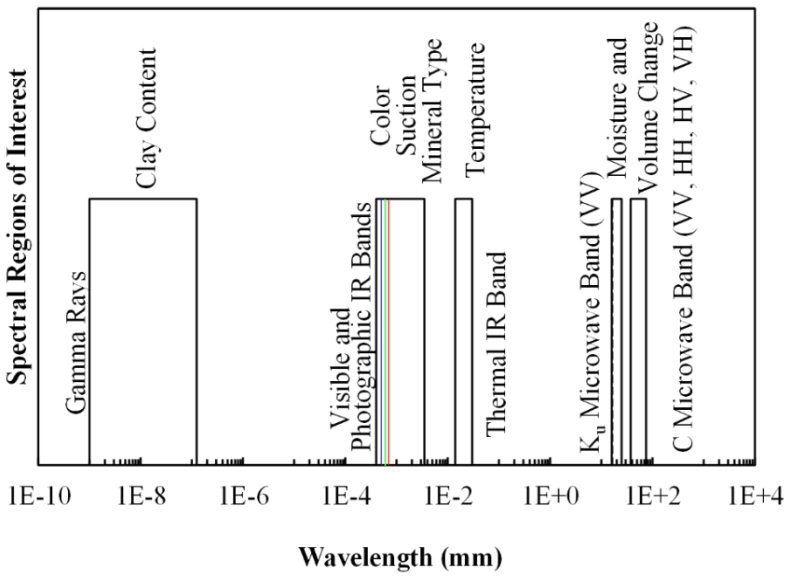

Figure 1.1. Spectral regions of interest for remote sensing of soils (modified from Coffman 2012).

Shepherd and Walsh 2002, Cozzolino and Moron 2003, Garner 2017). In almost all of the reviewed literature, the remote measurements were collected from dilute soil specimens in the laboratory.

Garner (2017) employed a Laser Analysis of Soil Tension (LAST) technique, using two low-power laser diodes and a high radiometric resolution spectroradiometer instrument (ASD FieldSpec 4 Hi-Res) to determine the soil moisture and soil water potential for dilute laboratory soil specimens. Two analytical methods were employed by Garner (2017). These methods included the Kubelka-Munk method (Kubelka and Munk 1931, Kubelka 1948) and the Beer-Lambert method (Stenberg and Viscarra Rossel 2010, Hapke 2012). Two empirical methods were also employed by Garner (2017). These empirical methods relied upon partial least squares or principle components regression techniques (Janik and Skjemstad 1995, Chang et al. 2001, Garner 2017). Garner (2017) concluded that the empirical methods outperformed the analytical solutions in predicting soil water potential. An example of an empirical remote sensing-derived soil water characteristic curve (SWCC) is presented as Figure 1.2.

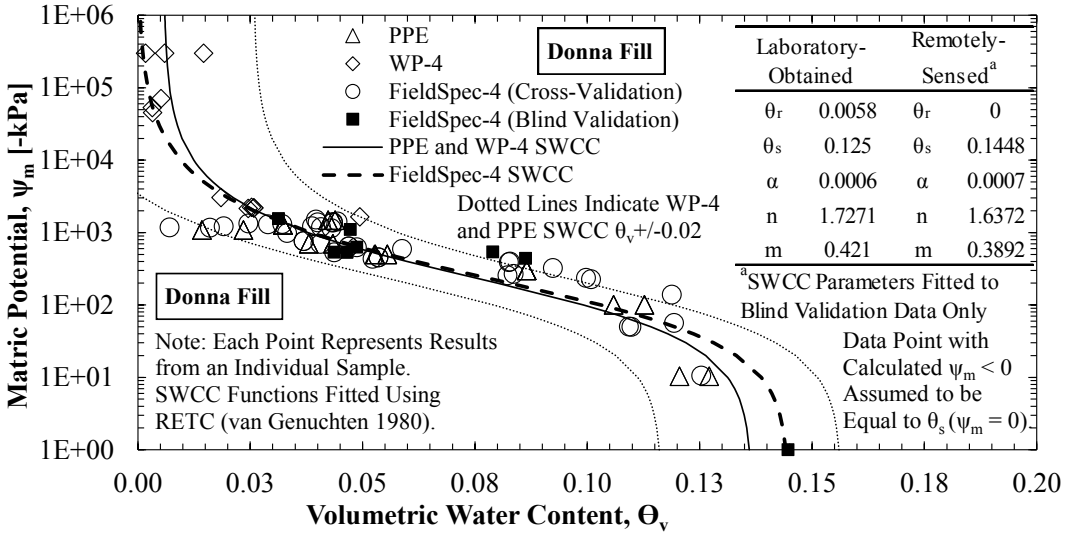

Figure. 1.2. Comparison of soil water characteristic curves (SWCC) derived from traditional laboratory techniques (pressure plate extractor [PPE] and WP4 dewpoint potentiometer [WP-4]) and from the reflectance spectroscopy technique using a FieldSpec-4 spectroradiometer instrument (from Garner 2017).

1.3.1. Lidar

Light Detection And Ranging (LIDAR), also referred to as Laser Detection And Ranging (LADAR), or in some cases laser radar, was coined by Middleton and Spilhaus (1953) and predated even the invention of the first lasers (Maiman 1960, McClung and Hellarth 1962). Modern lidar systems are rooted in the principles of radar technology but have matured as a technology that spans a wide range of applications from simple single-target ranging systems to systems used to identify atmospheric pollutants or wind speeds. The simplest form of the lidar equation relates the range distance to the target (*R*) to the

signal power of the backscattered light (P) by using Equations 1.1 through 1.6, as obtained from Collis and Russell (1976) and Wandinger (2005).

$$P(R) = K \cdot G(R) \cdot \beta(R) \cdot T(R) \quad \text{(Wandinger 2005)} \quad \text{[Eq. 1.1]}$$

$$K = P_0 \cdot \frac{c \cdot \tau}{2} \cdot A \cdot \eta \quad \text{(Wandinger 2005)} \quad \text{[Eq. 1.2]}$$

$$G(R) = \frac{\mathrm{O(R)}}{\mathrm{R^2}} \quad \text{(Wandinger 2005)} \quad \text{[Eq. 1.3]}$$

$$\beta(R) = \beta_{mol}(R) + \beta_{aer}(R) \quad \text{(Wandinger 2005)} \quad \text{[Eq. 1.4]}$$

$$T(R) = exp\left[-2 \int_0^R \alpha(r) dr\right] \quad \text{(Wandinger 2005)} \quad \text{[Eq. 1.5]}$$

$$P(R) = P_0 \cdot \left(\frac{c \cdot \tau}{2}\right) \beta(R) \cdot A \cdot R^{-2} \cdot \exp\left[-2 \int_0^R \alpha(r) dr\right] \quad \text{(Collis, Russell 1976)} \quad \text{[Eq. 1.6]}$$

In Equation 1.1, K is a constant that represents the efficiency of the system, G is the geometric range factor as a function of range, β is the backscatter coefficient at a distance R, and T represents the atmospheric transmission loss factor as a function of range. In Equation 1.2, P_0 is the average power of a single laser pulse, c is the speed of light, τ is the pulse length, A is the effective receiver area, and η is the system efficiency. In Equation 1.3, O is the overlap function as a function of range. In Equation 4, where β_{mol} is the molecular scattering index as a function of range and β_{aer} is the aerosol scattering index as a function of range. In Equation 1.5, α is the atmospheric extinction factor. In Equation 6, the atmospheric extinction factor, α, may be calculated as the sum of the water vapor absorption and all other scattering and absorption from atmospheric gases and particles ($\alpha = \alpha_{wv} + \alpha_A$), where the water vapor absorption coefficient is equal to the product of the absorption cross section, σ, and the number density of molecules, N ($\alpha_{wv} = \sigma N$).

Recent developments in lidar technology have included long-range lidar, low-peak-power and high repetition frequency lidar, hybrid lidar, and ultrafast lidar. Some lidar devices, like the Oppenheim and Menzies (1982) device, have aligned transmitters and receivers through an aperture, whereas others devices, like the Wallace et al. (2005) device, do not share a common aperture. Some lidar systems use pulsed lasers (Nehrir et al. (2012), while others emit continuous waveform (CW) lasers. There are also a variety of different carrier signal modulation techniques, including frequency, amplitude, phase, and polarization modulation. In addition to the various modulation techniques, a variety of detection schemes have been utlized, including direct, coherent, incoherent, heterodyne, and homodyne detection. Few differential absorption lidar systems have been built twice (Weitkamp 2005), because each lidar instrument has been developed for a specific purpose.

In recent years, frequency modulated, continuous waveform (FMCW) lidar has become popular for altimeter applications where low peak output power was obtained (Karlsson and Olsson 1999, Allen et al. 2001, Pierrottet et al. 2005, Pierrottet et al. 2008, Adany et al. 2009). Similar to radar systems, a pulse compression technique has been applied for the aforementioned FMCW systems, whereby a linear frequency sweep or "chirp" with a large bandwidth has been applied to the carrier signal modulation algorithm. Through this technique, high range accuracy was maintained, while the

bandwidth requirements of the receiver were reduced. For an FMCW lidar, the approximate range accuracy (σ_R) can be determined by using Equations 1.7 and 1.8.

$$\sigma_R = \frac{K_C}{B\sqrt{2 \cdot SNR}} \qquad \text{(Skolnik 1960, Jelalian 1992, Allen et al. 2001)} \qquad \text{[Eq. 1.7]}$$

$$SNR = \frac{P_{sig}}{P_{n-RX}} \; ; \; SNR_{coh} = \frac{\Re \cdot P_r}{2 \cdot q \cdot B_{RX}} \qquad \text{(Allen et al. 2001)} \qquad \text{[Eq. 1.8]}$$

In Equation 1.7, where K_C is a constant that is dependent on the chirp waveform, B is the signal bandwidth, and SNR is the signal to noise ratio of the receiver. In Equation 1.8, where P_{sig} is the detected signal power and $P_{n\text{-}RX}$ is the receiver noise power; SNR_{coh} is the signal to noise ratio for a shot-noise-dominant coherent detection process, $\Re$ is the photodetector responsivity, P_r is the received signal power, q is the electron charge ($1.6x10^{-10}$ C), and B_{RX} is the bandwidth of the receiver.

In the Adany et al. (2009) configuration, the FMCW lidar architecture was simplified by utilizing a modified, self-chirped, homodyne, coherent detection scheme. The frequency downconversion and de-chirping operations were completed within the photodetector of the received channel. The carrier signal was modulated and then split into two parts, where one part served as the reference signal, or local oscillator (LO), and the other part continued on to the system transmitter. The LO was sent directly to the receiver, a balanced photodetector (BPD). The received signal was also sent to the BPD. The coherent optical mixing between the LO and received optical signals occurred in the BPD. Using this technique, the range information was easily determined through FFT frequency analyses. The advantages of the simplified Adany et al. (2009) approach included the following list of items. 1) The process was used to eliminate the need to perform RF signal de-chirping. 2) The process enabled reduction in receiver bandwidth requirements. 3) The process helped to maintain high receiver sensitivity and range accuracy.

1.3.2. Differential Absorption Lidar (DIAL)

A specialized type of lidar, called Differential Absorption Lidar (DIAL) uses the physical process of absorption by atoms and molecular species in the atmosphere to determine their concentration. According to Bösenberg (1998) and Machol et al. (2004), unlike the coherent backscatter from a hard target (that is detected with conventional altimeter lidar instruments), the scattering of light within the atmosphere is incoherent and is characterized by elastic Rayleigh scattering from gases and Mie scattering from particles. Historically, DIAL instruments have been developed to determine atmospheric concentrations of gas and particle species through the use of vertical measurements. However, there are few examples of DIAL instruments being operated in non-vertical orientations (Nehrir 2011, Ishii et al. 2013). For DIAL measurements of water vapor concentration, two closely spaced wavelengths of laser light are transmitted through the atmosphere. One is called the on-line wavelength, which is heavily absorbed by water vapor, while the other is called the off-line wavelength, which is not absorbed by water vapor but is absorbed by free water (Figure 1.3).

The on-line and off-line lasers are pulsed intermittently along the same path. With short enough pulses, the difference in the measured returns from the on-line and off-line wavelengths should be only due to the absorption of the laser light by water vapor molecules. For this process to yield beneficial results, a spectral region of interest must be located in which the on-line and off-line wavelengths are adjacent. The temperature dependence of the DIAL measurements must also be reduced. Thus, various wavelength ranges have been recommended in the literature. Grant (1991) used wavelengths between 720-730 nm and Machol et al. (2004) used wavelength near 823 nm. The water vapor density averaged over distance, identified as $\rho_v(R)$, is calculated using Equations 1.9 and 1.10. The high-resolution transmission molecular absorption database, or HITRAN (Rothman 2013) is also used in this process. For vertical measurements of the atmospheric water vapor concentration, the Voigt function changes due to thermal- and pressure-broadening effects. These line-broadening effects are typically extrapolated from ground measurements and the water vapor density is calculated using Equations 1.11 and 1.12.

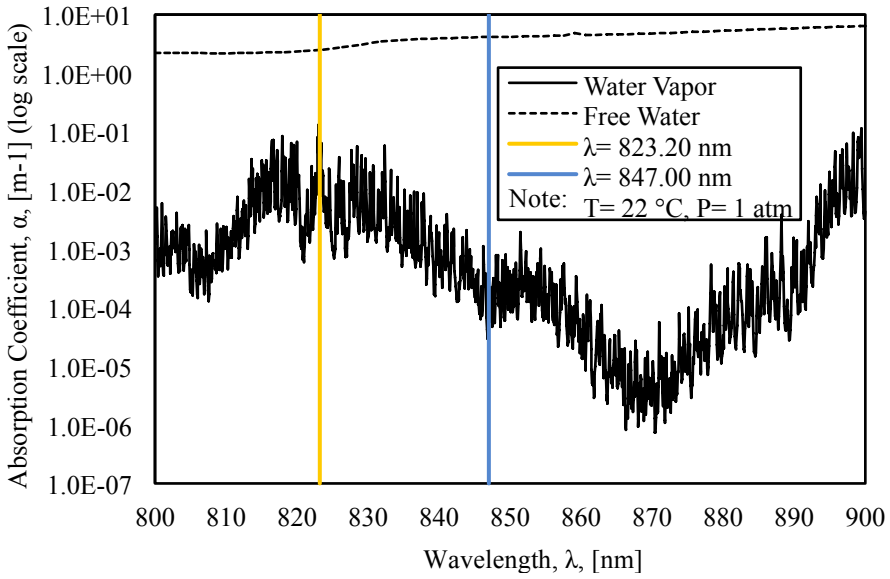

Figure. 1.3. Absorption coefficient as a function of wavelength for free water and water vapor with transposed on-line (823.20 nm) and off-line (847.00 nm) laser wavelengths (data: Kou et al. 1993, Pope and Fry 1997, Rothman et al. 2013).

$$\rho_v(R) = \frac{M_{H_2O}}{N_A} \cdot \frac{1}{2\cdot(\sigma_{on}-\sigma_{off})\cdot\Delta R} \cdot \left[ln \frac{P_{on}\cdot R\cdot P_{off}\cdot(R+\Delta R)}{P_{on}\cdot(R+\Delta R)\cdot P_{off}\cdot R}\right] \quad \text{(Schotland 1974)} \quad \text{[Eq. 1.9]}$$

$$S(T) = S_0 \cdot \left(\frac{T_0}{T}\right)^{1.5} \cdot exp\left[-\frac{h\cdot c\cdot E"}{k_B}\left(\frac{1}{T}-\frac{1}{T_0}\right)\right] \text{ (Bösenberg 1998, Ehret et al. 1993)} \text{[Eq. 1.10]}$$

$$\rho_v = \frac{e_s\cdot RH}{100\cdot R_v\cdot T} \quad \text{(Machol et al. 2004)} \quad \text{[Eq. 1.11]}$$

$$e_s = e_{s0} \cdot exp\left[\frac{L}{R_v}\left(\frac{1}{T_0}-\frac{1}{T}\right)\right] \quad \text{(Machol et al. 2004)} \quad \text{[Eq. 1.12]}$$

In Equation 1.9, M_{H2O} is the molecular weight of water, N_A is Avogadro's constant, σ_{on} and σ_{off} are the on-line and off-line water vapor absorption cross-sections ($\sigma=S\Lambda$, where S is the temperature dependent absorption line strength and Λ is the Voigt function), and P_{on} and P_{off} are received on-line and off-line backscatter signals. In Equation 1.10, S_0 and T_0 are the absorption line strength and temperature under standard conditions, h is the Planck constant, c is the speed of light, E" is the lower-state energy, and k_B is the Boltzmann constant. In Equation 1.11, e_s is the saturation vapor pressure (Equation 8), RH is the relative humidity ($RH \approx 100\frac{e}{e_s}$), $e=\rho_v R_v T$), and R_v is the water vapor gas constant equal to 461 J $kg^{-1}K^{-1}$. In Equation 1.12, e_{s0} is the saturation vapor pressure at $T_0=273$ K and is equal to 611 Pa, and L is the latent heat of vaporization and is equal to $2.5\times10^6\ Jkg^{-1}$.

DIAL theory was developed by Schotland (1966), but has been further developed over the last six decades (Schotland 1974, Menzies and Schumate 1976, Grant 1982, Grant 1991, Hardesty 1984, Bösenberg 1998, Wulfmeyer and Bösenberg 1998, Wulfmeyer and Walther 2001, Spuler et al. 2016). A variety of DIAL instruments and DIAL measurement techniques have been developed to measure tropospheric water vapor profiles. The platforms from which these measurements have been performed have included ground-based (Hardesty 1983, Prasad and Geiger 1996, Wulfmeyer 1998, Little and Papen 2001, Machol et al. 2004, Nehrir 2008, Nehrir 2011), airborne (Bufton et al. 1983, Ehret et al. 1993, Bruneau et al. 2001a, Bruneau et al. 2001b), and spaceborne platforms (Remsberg and Gordley 1978, Megie and Menzies 1980). When employed properly, the DIAL methodology has been the most accurate measurement of atmospheric water vapor concentration (Ismail and Browell 1989, Bösenberg 1998, Wulfmeyer and Walther 2001, Weckwerth et al. 2016).

A compact, ground-based DIAL instrument was developed by an interdisciplinary group of electrical and computer engineers at Montana State University (MSU) in Bozeman, Montana and has received continued improvements. These improvements include transmitter and receiver design, field adaptation, and even semi-automation (Nehrir 2008, Nehrir 2011, Nehrir et al. 2009, Nehrir et al. 2011, Nehrir et al. 2012, Repasky et al. 2013, Spuler et al. 2015, Spuler et al. 2016, Weckwerth et al. 2016). The DIAL instrument at MSU was designed for near-field and far-field observations of water vapor concentration within the troposphere with reported usable range from 0.5 km to 12 km.

Chapter 2: Development of Advanced Machine Learning Debris Flow Model

The use of advanced machine learning, for the development of a debris flow model, was described in a journal article that was developed by the project team. The manuscript, entitled, "Machine Learning Based Predictive Modeling of Debris Flow Probability Following Wildfire in the Intermountain Western United States" was written by Ashley Kern, Priscilla Addison and Thomas Oommen from Michigan Technological University and by Sean Salazar and Richard Coffman from the University of Arkansas. The paper was published in the Mathematical Geosciences journal. An electronic copy of the article is included as Appendix A of this document.

Chapter 3: Refinement of Advanced Machine Learning Debris Flow Model

A summary of efforts taken to develop probability models, to predict locations that are vulnerable to the occurrence post wildfire debris flow events, is provided in this chapter. Research in the area of probability models was pioneered by the USGS, where a logistic regression modeling approach was used to investigate relationships between descriptive characteristics of recently burned basins and the likelihood to produce debris flows. This work began in 2005 but there have been several refinements to the models over the years. Two dataset were published by the USGS to correspond to some of these model refinements. The first dataset was released in 2005; this dataset had 609 samples and 26 predictors. The second dataset was released in 2016; this dataset had 1550 samples and 26 predictors.

As mentioned earlier, all of the USGS that have been built over the years investigated only the logistic regression algorithm. The logistic regression algorithm is a linear algorithm, and thus only linear relationships between a given predictor and the corresponding response can be determined. However, the debris flow mechanism is a complex phenomena; the relationship between a given predictor and the corresponding response might best be captured by using nonlinear relationships. Machine learning algorithms, which afford the possibility of exploring the hypothesized nonlinear relationships between variables were therefore investigated. Machine learning algorithms offer flexibility through data driven predictions made by iteratively learning from the input data, as opposed to the strictly static algorithms of linear models. A comparison of the best models for the two datasets between the USGS approach and a machine learning approach are described in the next two paragraphs.

The first USGS dataset (the 2005 dataset) was used in a 2010 study by the USGS, which resulted in the best model yielding a sensitivity of 44-percent. This meant that the model was able to correctly predict four out of 10 potentially hazardous debris flow locations. Applying machine learning algorithms to this same dataset yielded a sensitivity of 72-percent, using the nonlinear Naïve Bayes model, which is almost a two-fold improvement. This sensitivity of 72-percent corresponds to seven out of 10 of the debris flow locations being correctly predicted. The use of machine learning showed great promise and gave credence to the hypothesis that the relationship between the data was likely nonlinear, as opposed to the linear approach recommended by the USGS.

A 2017 study, as completed by the USGS, still employed the logistic regression modeling approach rather than machine learning approaches. The 2017 study used a larger dataset (the 2016 dataset) and gave much improved results of 72-percent sensitivity. This meant that an approximate seven out of 10 of the hazardous debris flow locations could be potentially correctly predicted. The new model also gave a specificity of 58-percent meaning that an approximate six out 10 of the burned basins that were "safe" would be correctly isolated; therefore four out of 10 false alarms were incorrectly predicted as debris flow locations. Although this updated model provided an increased ability to predict potential debris flow events, it also holds the risk of desensitizing the public, as the low specificity value means there will be a high number of false positives

predicted. Applying the machine learning algorithms to this same dataset, using the C5.0 decision tree algorithm, yielded a sensitivity of 82-percent and a specificity of 82-percent, which indicates a balance of model efficacy. These results again give credence to the hypothesis that the relationship between the predictors and response variables is nonlinear, as the C5.0 decision tree is a nonlinear algorithm.

3.1. Overview of the Decision Tree Methodology

The dangers associated with a wildfire do not end after the wildfire is contained. A wildfire can increase the susceptibility to other secondary hazards such as flooding, rock falls, debris flows, etc. A debris flow is a fast-moving, high-density slurry of water, sediments and debris that travels under gravity and is endued with enormous destructive power (Cannon et al. 2010). Debris flows are on the higher risk side of the secondary hazard spectrum, because fatalities have been caused by post-fire debris flows, in a majority of incidences. Based on previous research, the vulnerability of a location to experience a post-wildfire debris flow can persist for an average of two years after the fire (Cannon and Degraff, 2009). With increasing wildfire frequencies in the western United States, researchers are working to supplement emergency response efforts to help alleviate the risks to these hazards. Work completed to date has been focused on developing predictive models that help isolate the locations within a burned area that are likely to produce debris flow events, so necessary mitigating efforts may be applied.

Generally, there are two different modeling approaches for predicting the likelihood of post-wildfire debris flow occurrences: deterministic (Hungr et al. 1984, Johnson et al. 1991) and probabilistic (Cannon et al. 2010, Staley et al. 2017). The probabilistic approach have been shown to be advantageous over the deterministic counterpart since a probabilistic approach 1) provides objective and satisfactory results even with incomplete or low quality datasets, 2) allows inputs to be treated stochastically, and 3) provides valuable information for risk analyses (Hammond et al. 1991, Donovan and Santi 2017). Researchers at the United States Geological Survey (USGS) have spearheaded work on the probabilistic approach using dataset with descriptive characteristics on past debris flow events such as basin morphology, burn severity, rainfall characteristics and soil properties to build logistic regression models that predict the statistical likelihood of post-fire debris flow occurrence in western United States (Canon et al. 2010, Staley et al. 2013, Staley et al. 2017). This work began in 2005 but there have been several refinements to the models over the years (Cannon and Gartner 2005, Cannon et al. 2010, Staley et al. 2017). The logistic regression approach is advantageous, mostly because it is the most universally known classifier that considers simple linear relationships that are computationally simple and easy to interpret. However, the simplicity is also disadvantageous because a debris flow is such a complex phenomenon whose full mechanics are not even fully known to date (Cannon et al. 2010). This complex nature of debris flow mechanics gives rise to the analogy that best performance of a predictive model cannot be achieved by considering only simplified linear relationships. The use of machine learning algorithms, which afford the possibility of exploring the hypothesized nonlinear relationships between variables was therefore utilized for this project. Machine learning algorithms offered flexibility through data

driven predictions made by iteratively learning from the input data, as opposed to the strictly static algorithms of some linear models. As previously mentioned, the USGS has released two sets of datasets to correspond to some of the model refinements over the years; these datasets were investigated for this USDOT project. The first dataset, released in 2005, had 609 samples and 26 predictors (Gartner et al. 2005). The second dataset, released in 2016, had 1550 samples and 26 predictors (Staley et al. 2016).

A subset of the first dataset (the 2005 dataset) was used in a 2010 study by the USGS, which resulted in their best model built for the Intermountain USA yielding a sensitivity of 44-percent. This meant that the model was able to correctly predict four out of 10 of these potentially hazardous debris flow locations. Applying machine learning algorithms to this same dataset, three regional subsets were considered: the entire western USA, Southern California, and Intermountain west USA (Figure 3.1). The results showed that Southern California, by virtue of the scarcity data, gave the worst results. The combined western USA model gave average results, and the intermountain west model gave the best results of 72-percent sensitivity using the nonlinear Naïve Bayes algorithm. This is almost a two-fold improvement on the logistic regression approach and corresponds to an improved ability to correctly predict seven out of 10 debris flow locations.

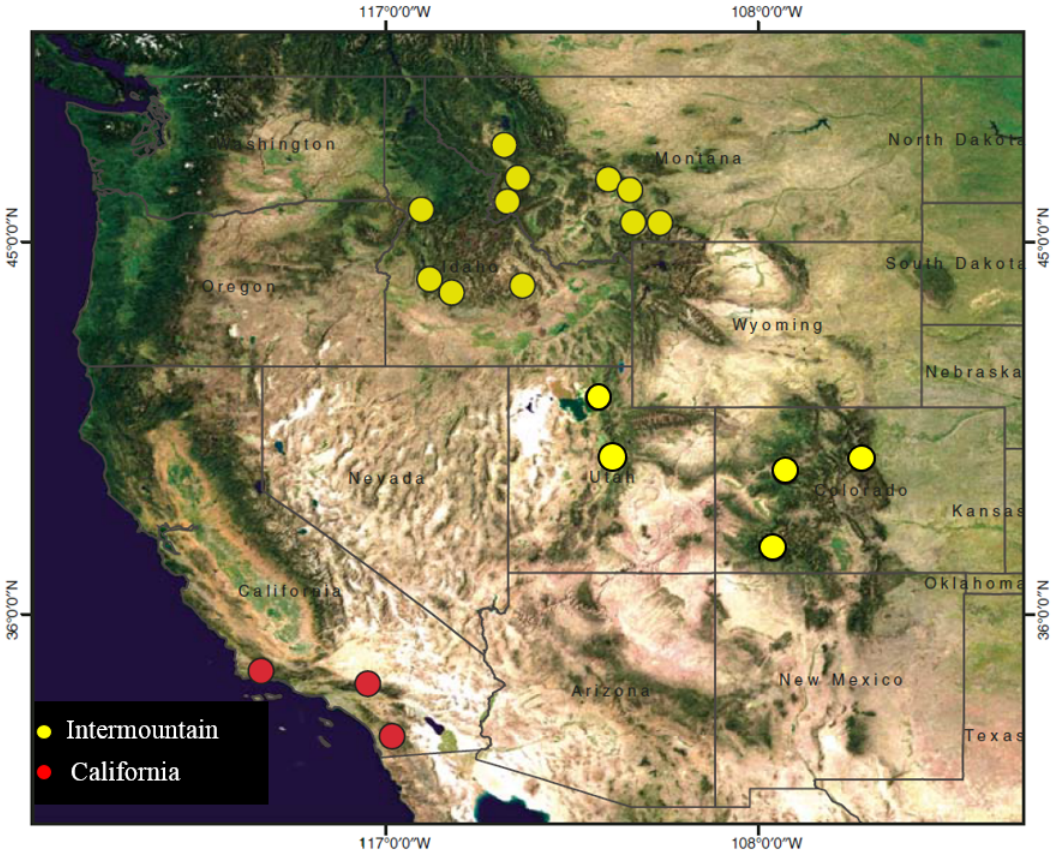

Figure 3 1. Locations of data associated with Intermountain west USA (yellow dots) and Southern California (red dots) (adapted from Cannon et al. 2010).

Based on the results, the local geography had an influence on predictive capability of the output model. However, the model was still applicable for Southern California, as the model was used for a back analyses of the October 15, 2015 event in Los Angeles County that resulted in one fatality and took out 40-mile sections of the I-5. The 2015 I-5 event was believed to have been triggered from a 2013 fire that occurred at this location. The output showed that the Naïve Bayes model predicted a probability of 60-100% of debris flow occurrence, if a 5-year storm occurred (Figure 3.2). This showed that the model, which was created for the intermountain West, was robust enough to be applied to Southern California. Results from the model development and validation has been summarized and presented in a publication titled: "Machine Learning Based Predictive Modeling of Debris Flow Probability Following Wildfire in the Intermountain Western United States" in the Mathematical Geosciences journal (Kern et al. 2017 - full manuscript in Appendix A). The overall results also showed great promise and gave credence to the hypothesis that the relationship between the data was likely nonlinear as opposed to the proposed linear USGS approach.

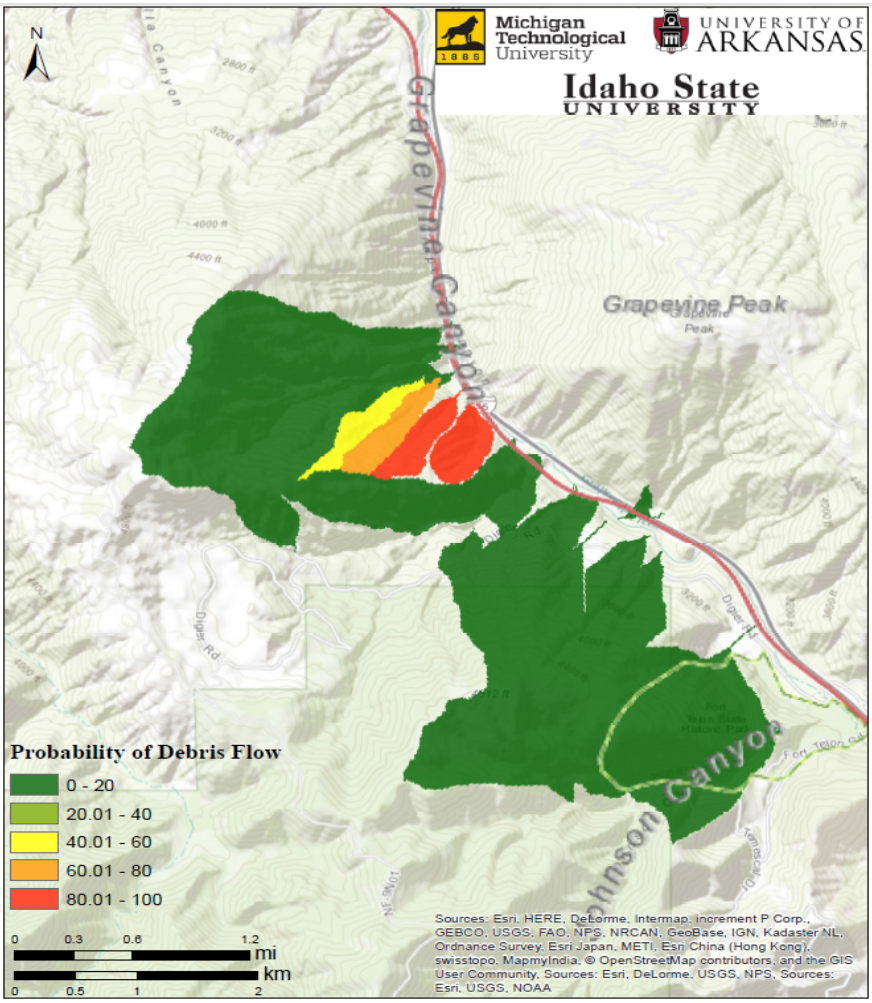

Figure 3.2. Estimated probability of post-wildfire debris flows in the area burned by the 2013 Rancho fire in California based on a 5-year- recurrence rainfall data.

The larger second dataset (the 2016 dataset) was used in a 2017 study by the USGS. During the 2017 study, the USGS still employed the logistic regression modeling approach. Much improved validation metrics were obtained from the 2017 study. A sensitivity of 72-percent was obtained, which meant that an approximate seven out of 10 of these hazardous locations could now be potentially correctly predicted. The new model also gave a specificity of 58-percent, meaning that an approximate six out 10 of burned locations that were "safe" were correctly isolated; therefore debris flow was incorrectly predicted at four out of every ten of the sites. Although this updated model provided an increased ability, as compared with the 2010 USGS model, false prediction of potential debris flow events may desensitize the public, as a low specificity value means there will be a high number of false positives predicted. As part oft the USDOT project that is described herein, the C5.0 decision tree algorithm was investigated by applying the machine learning algorithms to this same dataset. This decision tree method was used because, although the Naïve Bayes algorithm used in the earlier study, and though the Naïve Bayes algorithm is robust the inner workings of the model are unknown. Simply put, the Naïve Bayes algorithm did not offer much insight into the relationships of the predictors, as they relate to the response. The nonlinear tree based algorithm of the C5.0 model, on the other hand, is simplified and transparent. The algorithm works by splitting the dataset into smaller, more homogeneous, groups. The C5.0 model works in a flowchart manner whereby stepwise decisions are made on predictors at different levels to iteratively determine unique breakpoints as they relate to the different classes of the response variable. This robust, yet simple model yielded a sensitivity of 82-percent and a specificity of 82-percent, which is a balance of model efficacy. The results of this study have been summarized in a manuscript titled: "*Assessment of post-wildfire debris flow occurrence using classification classifier tree*" that has been submitted to a peer-reviewed journal for review and publication. This manuscript is included as Appendix B of this final report.

Since the beginning of this project, different agencies have requested predictions for recently burned areas in the jurisdiction of the given agency. To date, twenty (20) model prediction outputs, across six states, over the past two years, have been developed. Screenshots of these predictions are included in Appendix D of this report but interactive copies can also be found on the NASA RECOVER platform (http://giscenter.isu.edu/Research/Techpg/nasa_RECOVER/index.htm) as well as the website for the project (http://wildfire-landslide-risk-dss.uark.edu/models/). Initially, it took approximately three days to produce these model outputs; now with a streamlined process, an average of five hours is spent to develop a given model. The streamlined process included building a semi-automated model to extract the needed data of the fire-affected site.

3.2. Submitted Journal Article on Decision Tree Methodology

The use of advanced machine learning, for the development of a debris flow model, was described in a submitted journal article that was developed by the project team. The manuscript, entitled, "Assessment of Post-Wildfire Debris Flow Occurance Using Classifer Tree" was written by Priscilla Addison, Thomas Oommen, and Qiuying Sha from Michigan Technological University. The paper is currently under review in Geomorphology. An electronic copy of the article is included as Appendix B of this document.

Chapter 4: Radar Remote Determination of Soil Properties

The determination of the volumetric water content of soil, by using the Gamma Remote Sensing Portable Radar Interferometer – Version II module of the Soil Observation Topographic Differential Absorption Lidar (SOTDiAL) module, was described in a journal article that was developed by members of the project team. The manuscript, entitled, "Volumetric Water Content as Obtained from Remote Sensing and In-Situ Instrumentation" was written by Cyrus Garner and Richard Coffman from the University of Arkansas. An electronic copy of the article is included as Appendix C of this document.

Chapter 5: Optical Remote Determination of Soil Properties

The determination of soil properties from remote sensing methods, was described in a conference proceeding that was developed by the project team. The manuscript, entitled, "Evaluation of a Field and Laboratory Remote Sensing Method for Determining Atterberg Limits and Clay Content" was written by Cyrus Garner, Sean Salazar, and Richard Coffman from the University of Arkansas. The paper was submitted to the Transportation Research Board (TRB), but was not published. Because the article was not published, the text from the article has been formatted to be a part of this document and is included in this chapter. A modified version of the TRB manuscript, entitled "Index and Hydraulic Properties of Soil Using Visible Through Near-infrared Spectroscopy" was submitted to *Soil Science.*

5.1. Abstract

Remote measurement of soil index properties (liquid limit and plastic limit) and clay content offer potential benefits over traditional laboratory testing. The techniques presented herein allow for rapid, repeatable, and non-destructive collection and processing of data. Soil spectroscopy was utilized in the visible to near infrared spectrum and in the mid infrared spectrum in the laboratory setting to derive liquid limit, plastic limit, and clay content for three silt soils. Reflectance spectra from each of the soils were analyzed using partial least square and principle components regression techniques. A comparison of the spectroscopy results with results obtained from traditional, standard of practice laboratory methods indicated that the variability of the liquid limit, plastic limit, and clay content parameters was similar. Additionally, the mineralogy of two of the three soils that were tested was evaluated through a correlation with reflectance spectra. The mineralogical classifications were verified using x-ray diffraction and scanning electron microscope procedures. Based on the acceptable precision of the presented techniques, it is suggested that the remote measurement and characterization of soils offer a viable supplement or alternative to traditional techniques currently employed by engineering professionals in the field. Using visible near infrared spectroscopy on intact soil samples, the bias between remotely sensed and traditionally obtained values of liquid limit, plastic limit, and clay fraction were less than 1 percentage point. Similarly, the maximum standard deviation of the remotely sensed properties were 2.4, 0.6, and 5.1 percentage points for the liquid limit, plastic limit, and clay fraction, respectively.

5.2. Introduction

A remote measurement technique for determining Atterberg limits (liquid limit and plastic limit) as well as the mass fraction of clay was evaluated. Specifically, the suitability of utilizing visible to near infrared (VisNIR) and mid-infrared (MIR) spectroscopy for the measurement of index properties was investigated. Both ground, oven dry, soil samples (VisNIR-Dry and MIR-Dry) and intact, wet soil samples (VisNIR-Wet) were investigated. The reflectance and index properties of three separate silty soils were considered due to the prevalence of these soil types in transportation projects within

the state of Arkansas. Soil samples were acquired either commercial suppliers (Donna Fill Company and the Thiele Kaolin Company) or directly from a field site.

Soil index properties, specifically, the liquid limit (LL) and plastic limit (PL), as well as clay content (CF), are often important parameters that must be considered during the design of transportation. Specifically, the PL and CF are used to evaluate soil mineralogy and classify the soil using the Unified Soil Classification System (USCS). However, traditional laboratory testing including the use of the Casagrande drop cup (1), the rolling method (1), the fall cone (2), and the hydrometer (ASTM D422 [1]) are spatially limited, labor intensive, time consuming, and have been reported to be poorly repeatable (3,4). Reflectance spectroscopy has the potential to provide a method to acquire spatially vast, near real time measurements of soil index properties and clay content (5).

For transportation and geotechnical engineering applications, increased spatial extent will allow designers to gain a more comprehensive understanding of the various soil types and the locations of those soil types on a project or regional scale. The advantages of the proposed method include allowing engineering professionals to non-destructively acquire near real time values for index properties of samples recovered during geotechnical explorations. The aforementioned remotely sensed index properties will then be used to identify areas of increased concern or be used to optimize sampling and testing methods. Since the proposed method is non-destructive, samples that have been tested can be used for further testing (e.g. direct shear, triaxial compression).

Contained in this document is a review of the limitations of traditional methods of obtaining soil index values and previous investigations of VisNIR and MIR spectroscopy in soil science (Section 5.3). The soils investigated for this work, sample preparation techniques, the traditional laboratory techniques employed to obtain soil index values, the VisNIR and MIR instrumentation and techniques employed to acquire spectral data, and the statistical techniques employed to obtain empirical correlations between the measured soil index values and the reflectance spectra is presented and discussed in Section 5.4. The performance of each empirical correlation between liquid limit, plastic limit, and clay fraction for both VisNIR and MIR spectral data is presented and compared in Section 5.5. Finally, recommendations for the use of reflectance spectroscopy is presented (Section 5.6).

5.3. Review of Existing Methods

Atterberg limit values have been commonly used by geotechnical engineers to calculate engineering values in the absence of direct measurements (3,6). Specifically, the liquid limit (LL) and the plastic limit (PL) values have been used to provide an estimate of the coefficient of consolidation (7), permeability (8), normalized void ratio (9), and shear strength (3,10,11). However, the use of traditional laboratory testing techniques to determine index properties is time consuming because: 1) the samples must be transported from the field to the laboratory; 2) the samples must be prepared for testing (e.g. allow to soak or dry as required by ASTM D422 and ASTM D4318 [1]); 3) tests

must be conducted; and 4) tests typically require that the sample water content be determined by oven drying overnight. Furthermore, such tests are often time consuming to perform. For example, the traditional determination of LL and PL values require the samples to be oven dried for a period of 12-16 hours to determine the water content of the samples after testing (1,2). Similarly, the measurement of clay fraction (CF) requires 24 hours to complete (ASTM D422[1]). All of the aforementioned laboratory tests are destructive tests and the soil samples should not be reused for additional testing. In addition to the time consuming nature of the tests, another disadvantage is that the LL and PL tests, in particular, have been widely reported to be poorly repeatable (3, 4, 12, 13, 14).

Vis-NIR (400 to 2500 nm) reflectance techniques have been widely employed in agricultural, biological, ecological, and geological research. However, these techniques have not yet been largely adopted by design professionals within the transportation, geotechnical, or geonvironmental engineering fields. Soil properties that have been of interest to transportation professionals that have been measured using reflectance techniques include pH (15, 16, 17, 18, 19), clay content (4, 15, 16, 20, 21, 22), sand content (15, 16, 18), silt content (4, 15, 16, 18), and index properties (14, 23). In addition to the user of VisNIR, MIR (2500 to 25000 nm) techniques have been also been evaluated by previous researchers (5, 24). Most of the MIR and VisNIR testing previously conducted has been performed on dry, ground samples. The use of ground, dry samples results in testing methods are more time consuming and prevent the samples from being reused for additional testing. However, some research has been conducted on obtaining measurements of soil properties from soil samples in an in-situ condition. The in-situ measurements have included soils with variable moisture content (21, 25, 26) and soil structure (27, 17, 19, 28, 29).

To analyze the aforementioned VisNIR and MIR data, the partial least squares (PLS) and principle component analysis regression (PCR) have been widely employed (30, 31, and 32). Specifically, these multivariate techniques are well suited for analyzed large data sets (e.g. a spectra with many wavelength values) or varying correlation to the desired properties. Although both of the statistical techniques are robust, the PLS technique, in particular, has been employed reflectance spectroscopy for studies on soil (4, 5).

5.4. Methods and Materials

5.4.1. Soil Types Investigated

Three different soil types were investigated using both laboratory, MIR, and VisNIR techniques including: 1) a commercial kaolinite product ("Kaowhite-S") that was obtained from the Thiele Kaolin Company of Sandersonville, Georgia; 2) an illite clayey silt material that was obtained from the Blackhawk Coal Mine (Randolph County, Illinois) that is owned and operated by the Knighthawk Coal Company; and 3) an artificial nepheline syenite granite silt that was obtained from the Donna Fill Company (Little Rock, Arkansas). The bulk soil samples (as received from the manufacturer or

recovered from the field) were pre-processed prior to conducting any laboratory investigation. Specifically, the bulk soil samples were placed in a temperature controlled oven (105 +/- 5 °C) until dry and any large soil clods were then mechanically broken and ground. Following drying and grinding, the oven-dry, ground, soil was then sieved through a U.S. standard number 200 sieve (0.0075 mm nominal opening size) to remove any sand particles.

5.4.2. Laboratory Investigation of Soil Properties

Traditional laboratory techniques were employed to both characterize the soil and measure the soil index properties for use in the empirical correlation with the observed spectral data. Soil samples were characterized to obtain quantitative and qualitative measurements of CF (ASTM D422 [1]), mineralogy (x-ray diffraction, scanning electron microscopy, Terzaghi et al. [33]), LL (1, 2), PL (1, 2), and specific gravity (ASTM D854 [1]). All of the traditional laboratory tests were performed in sets of five and the average values were reported. The fall cone testing was performed procedures documented in BSI 1377 (2), while the X-ray diffraction (XRD) and scanning electron microscopy (SEM) were performed by the University of Arkansas Nano-Bio Materials Characterization Center.

5.4.3. Sample Preparation for Reflectance Testing

The samples that were to be tested using either VisNIR or MIR spectroscopy were maintained in either a desiccator or again placed in the oven prior to testing. For VisNIR-Dry samples, approximately 500 grams of dry ground soil was obtained from the previously prepared ground, dry soil stockpile. The samples were then placed into metal tins, with a volume of 240 ml, and oven-dried overnight prior to testing. The metal tins were removed from the oven, covered, and allowed to cool for one hour prior to testing. The VisNIR-Dry samples were removed from the larger metal tin and placed into a stainless steel sample cups each with a volume of 10 cm^3. Each sample was lightly pressed into the sample cup and struck off flush with the top of the sample container to ensure both a consistent sample volume and a consistent distance from the optics of the spectrometer. The MIR-Dry testing was performed at the Arkansas Center for Space and Planetary Sciences (ACSPS). The MIR samples were segregated into lots of 5 g (one for each spectral test) and were placed into stainless steel, each with a volume of 10 cm^3, sample cups and transported to the ACSPS in a sealed 250 ml glass desiccator that also contained with anhydrous calcium chloride. The samples were maintained in the sealed desiccator and only removed immediately prior to testing in order to prevent contamination of the sample by the absorption of atmospheric moisture.

The intact, unsaturated VisNIR-Wet samples were prepared using a multi-step method. Approximately, 800 grams of oven-dried ground soil was obtained from the previously prepared bulk samples and mixed into a slurry. The slurries, for the various soils, were mixed at gravimetric water contents of 50 percent (Donna Fill), and 75 percent (kaolinite and illite) in two batches (400 grams of dry soil each). The soil slurries were then consolidated using a double drained 6.4 cm diameter acrylic slurry

consolidometer under a constant applied stress of 138 kPa using an aluminum load frame. The applied stress was maintained until 48 hours beyond the end of primary consolidation (t_{100} + 48 h). The end of primary consolidation (t_{100}) was determined using the methods described in Fadum and Casagrande (34) and Taylor (35). After consolidation was complete, the consolidometer was disassembled and the acrylic cylinder, containing the saturated soil sample, was placed onto a 1.5 cm tall, 6.4 cm diameter acrylic sample ring. A smooth glass plate was placed under the sample ring and the sample was extruded from the consolidometer cylinder by applying a load to the aluminum load frame. The load was maintained until the sample had extruded enough to fill the 1.5 cm tall acrylic ring. The process was then repeated as each of the individual samples were removed from the soil column. Approximately eight samples were acquired from each soil columns.

Following being placed into the 1.5 cm tall rings, the soil samples and rings were then placed into a pressure plate extractor (PPE). Two PPE devices were employed to create samples with different levels of soil water potential. A laboratory pressure panel was utilized to monitor and control a 0-500 kPa PPE and a 0-1500 kPa PPE was supplied with a standalone high pressure air cylinder using a one–stage CGA-580 regulator was utilized to supply and control a 0-1500 PPE. The applied pressure, for both devices, was monitored using a Trautwein pressure transducer and electronic readout. The PPE samples were allowed to equilibrate with the applied pneumatic pressure until the volume of the expelled water from the PPE was less than 1 ml over a 48 period. After the samples attained the prescribed flowrate, the samples were subsequently removed from the PPE for use in reflectance testing.

5.4.4. Middle Infrared and Visible Infrared Spectroscopic Instruments

Two separate instruments were utilized to obtain spectral data from the VisNIR (400 to 2500 nm) and MIR (2500 to 25000 nm) wavelength ranges. A Nicolet 6700 Fourier Transform Infrared (FT-IR) spectrometer owned and operated by the ACSPS, with a diffuse reflectance accessory, was employed for all MIR testing. The instrument was controlled with the OMNIC software suite (36). As per instruction manual for the instrument (Nicolet 2004), the spectrometer was configured for use in the MIR wavelength range. A thermo-electrically cooled dueterated triglycine sulfate detector with a potassium chloride window (DTGS-KBR) and KBr beam splitter was employed (detection range between 7,400 and 350 cm^{-1}). The sample slide (0.25 cm^3 volume) was used to hold the sample during testing. An InfraGold (a trade name for an electrochemically plated diffuse gold-metallic coating) reference disk was used to acquire a background reflectance. The sample illumination was provided by an Ever-Glo ETC MIR source (36).

Visible-Near Infrared spectral data was obtained using an ASD PANalytical FieldSpec4 Hi-Res Spectroradiometer (FS4) owned and operated by the University of Arkansas College of Engineering. A Lenovo ThinkPad X1, using the RS^3 software suite, (37) was used to control the instrument, store the acquired spectral data, and perform preprocessing and data export. An eight degree instantaneous field of view fore optic was

employed to collimate the reflected light into the multi-mode fiber optic probe. A pistol-grip mount and a small tripod were used to ensure consistent positioning of the fiber optic probe relative to soil surface (or reference material). Reference spectra were collected using a 7.62 mm diameter Spectralon (a trade name for polyfluorethylene [PTFE] polymer). Sample illumination was provide using a 70 w quartz-tungsten-halogen bulb with an integrated reflector (ASD Illuminator Reflectance Lamp). A typical instrument set up for the laboratory testing is presented in Figure 5.1.

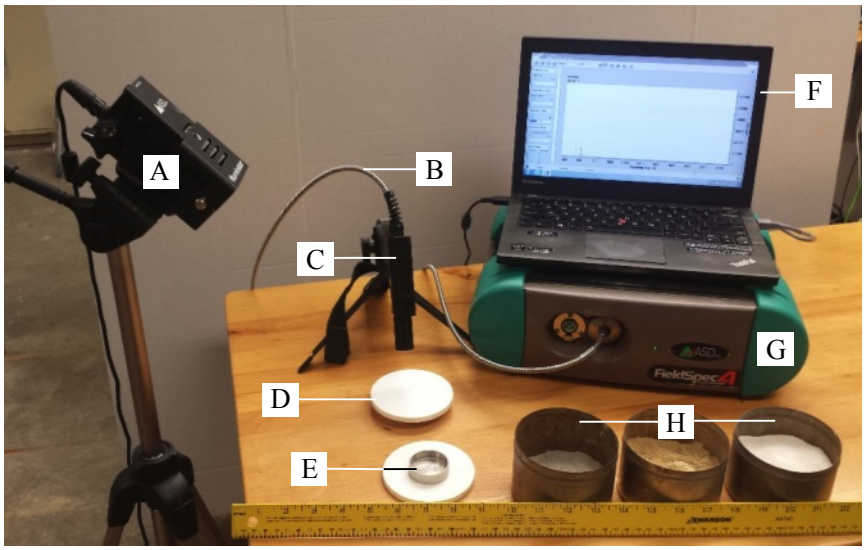

A. Halogen illumination source.
B. Fiber optic cable.
C. Fore optics (eight degree field of view).
D. 7.62 cm diameter Spectralon reference sample.
E. 10 cm^3 Steel Sample holder.
F. Laptop for data acquisition.
G. FieldSpec4 high resolution spectroradiometer (350-2500 nm)
H. Oven-dried soil samples (from left to right: Donna Fill, illite, kaolinite).

Figure 5.1 FieldSpec4 VisNIR spectroramadiometer and associated accessories (ruler shown for scale).

5.4.5. Collection of Reflectance Data

The FS4 spectrometer was allowed to warm up for at least 30 minutes prior to the acquisition of data. To remove spectral contamination, all of the overhead lights within the laboratory, were switched off prior to collection of data. The instrument settings were optimized using the RS3 software to maximize sensitivity and prevent saturation. Background reflectance (Spectralon) spectra were acquired before each soil sample and. Integration times between 16 and 128 mS were employed for spectral acquisition. For each sample, ten sets of ten spectra were computed and stored. Following the acquisition of the background spectrum, Vis-NIR samples were placed on the laboratory bench in the field of view of the instrument. For the intact samples, a 50mW 826 nm diode laser was used to orient the fore optic relative to the sample. Proper orientation was necessary for

some samples to avoid imaging large surface features such as cracking or uneven surface texture. Alignment was verified by illuminating a suitable area of the sample with the laser and adjusting the fore optic until the instrument detected a strong response at 826 nm. Spectrum acquisition was then conducted automatically for ten spectra with a one second delay between each acquisition. For the intact samples, at least two sets of ten spectra were acquired with the sample rotated by 90 degrees between acquisitions to mitigate directional effects on the spectra. The spectrum files were exported to tab delimitated text files, by using the ASD ViewSpecPro software suite (37). A total of 21 VisNIR-Dry spectra (8 for each soil) and VisNIR-Wet 72 spectra (30 kaolinite spectra, 32 illite spectra, and 8 Donna Fill spectra) were acquired.

MIR spectral data were acquired using the previously described Nicolet 6700 FT-IR device. Instrument function and configuration was confirmed using the onboard diagnostics prior to the collection of spectral data. Five gram lots of sample were removed from the glass desiccator and placed into the 0.25 cm^3 sample slide. The sample slide was then inserted into the instrument. A reference background reflectance spectrum was collected by sliding the sample holder out approximately 2.5 cm until the InfraGold reference sample was in the beam path. Background spectra were stored (using the OMNIC software) for use in preprocessing of the data prior to the collection of data for each spectrum. Spectral data were collected, with a (wavenumber) resolution of 1 cm^{-1}, and were averaged over 256 sequential acquisitions. The OMNIC software was also used to preprocess the data (convert the raw intensity to reflectance) and to export the reflectance spectra as a two column (wave number and reflectance) comma separated value (.csv) file. A total of 21 MIR-Dry spectra were acquired (5 kaolinite, 9 illite, and 9 Donna Fill).

5.4.6. Data Ingestion, Spectral Averaging and Statistical Data Analysis

All numerical analysis of the observed spectral data was performed using the MATLAB software suite (38). VisNIR spectral files for each sample were averaged (taking the arithmetic mean of the reflectance intensity at each wavelength for all spectra acquired for a sample). Specifically, MIR datasets were ingested, converted from wavenumber (k cm^{-1}) to wavelength (λ nm), and reordered. The empirical correlation between the measured engineering index values (LL, PL, CF) and the observed spectral data (wavelength and intensity) was determined using the MATLAB software. Both the partial least squares (PLS) regression techniques and the principle components (PCR) regression technique were performed using the MATLAB Statistics and Machine Learning Toolbox (for PLS) and Multivariate Data Analysis Toolbox (for PCR). Specifically, the plsregress.m (39) PLS executable and pca.m PCR executable (40) were utilized. The PLS regression was conducted using the straightforward implementation of a statistically inspired modification of the PLS method (SIMPLS) as proposed in (30) and further described in (32). For each data set, approximately 70 percent of the observed data was used to generate the regression. The remaining 30 percent of observed data was reserved for use as a validation data set. A total of 15 VisNIR-Dry spectra (5 for each soil), 45 VisNIR-Wet (19 kaolinite, 21 illite, and 4 Donna Fill), and 20 MIR-Dry (4 kaolinite, 8 illite, and 8 Donna Fill) were included in the individual calibration sets.

Conversely, a total of 9 VisNIR-Dry (3 for each soil), 25 VisNIR-Wet (11 kaolinite, 11 illite, and 3 Donna Fill), and 3 MIR-Dry (1 for each soil) were included in the individual validation sets.

Spectral reflectance intensities were stored in the X (n by p) matrix where n was the number of spectra in the calibration data set and p was the number of wavelength values in each spectrum. Measured values of each engineering index values (for n observations) were ingested and stored as the Y (n by 1) vector. An example of the Y and X matrix showing relative dimensions is presented in Figure 5.2.

LL	λ_1	λ_2	λ_3	λ_4	…	…	λ_{n-1}	λ_{n-1}	λ_{n-1}	λ_n	
31.5	0.89	0.89	0.89	0.89	0.89	0.89	0.89	0.88	0.88	0.88	< **Spectra1**
31.5	0.89	0.89	0.89	0.89	0.89	0.88	0.88	0.88	0.88	0.88	< **Spectra2**
31.5	0.45	0.45	0.44	0.44	0.44	0.44	0.44	0.44	0.44	0.44	< **Spectra3**
46.7	0.73	0.73	0.73	0.73	0.73	0.73	0.73	0.73	0.73	0.73	< **Spectra4**
46.7	0.72	0.72	0.72	0.72	0.72	0.72	0.72	0.72	0.72	0.72	< **Spectra5**
46.7	0.72	0.72	0.72	0.72	0.72	0.72	0.72	0.72	0.72	0.72	< **Spectra6**
25.0	0.46	0.46	0.46	0.46	0.46	0.46	0.46	0.46	0.46	0.46	< **Spectra7**
25.0	0.45	0.45	0.45	0.45	0.45	0.46	0.46	0.46	0.46	0.46	< **Spectra8**
25.0	0.47	0.47	0.47	0.47	0.47	0.47	0.47	0.47	0.47	0.47	< **Spectra9**
Y	**X**										

Figure 5.2. Example X and Y matrix for used in PLS and PCR regression.

The number of components for in the regression (N_c) was determined by evaluating the percent variance in **Y** that was explained at each value of N_c. As suggested in the MATLAB documentation (38), a maximum of 10 PLS or PCR components were considered. The value of N_c was selected to explain greater than 90 percent of the variation in **Y**. For the PLS and PCR regressions, two methods of validation were employed. A K-fold (ten folds) cross-validation procedure was employed to measure the estimated mean squared predictive error (EMSPE) value for each model as a function of Nc. Additionally, a subset (approximately 30 percent of the total number of samples acquired) of the original data set was excluded from the regression (calibration) data set. After selecting an appropriate value of N_c, the computed vector containing the PLS regression weighting coefficients (**β** vector) was subsequently employed to predict values of the index properties ($\mathbf{Y_{pred}}$) from the observed reflectance spectrum of the validation data set by using Equation 5.1.

$$Y_{pred} = X_{validation} \cdot \beta + F \qquad (31) \qquad \text{Equation 5.1}$$

*Where $\mathbf{Y}_{pred}$ is a vector (a by 1 one column), $X_{validation}$ is the matrix containing the observed reflectance spectrum (a rows by b columns), where a is the number of acquired spectra, b is the number of wavelength values in each spectra, and **F** is a one by one vector containing the Y-residual value.*

5.5. Results

5.5.1. Results Obtained from Traditional Laboratory Testing

As obtained using the ASTM D4318 (1) method, The LL values for each of the three soil types were determined to be 31.5 percent, 46.7 percent, and 25.0 percent for the kaolinite, illite, and Donna Fill material, respectively. Whereas the LL that was determined using the fall cone for the three soil types was 37.1 percent, 51.3 percent, and 36.0 percent for kaolinite, illite, and Donna Fill, respectively. The PL values for the kaolinite soil was determined to be 28.1 and 9.5 percent, as obtained by ASTM D4318 (1) and the fall cone method, respectively. The PL values for the illite soil was determined to be 23.6 and 30.2 percent, as obtained by ASTM D4318 (1) and the fall cone method, respectively. The Donna Fill material was determined to be non-plastic by both the ASTM D4318 (1) and the fall cone method. Each of the three soil types were characterized as silt materials with a clay fraction of 47.2 (kaolinite), 46.5 (illite), and 8.9 (Donna Fill) percent, respectively (Figure 5.3).

The mineralogy of the kaolinite and illite materials was experimentally validated using the XRD testing results (Figure 5.3). Similarly, the clay mineralogy was also qualitatively validated with 1) the empirical method proposed in (40) and 2) the SEM imagery for the kaolinite and illite material (Figure 5.4).

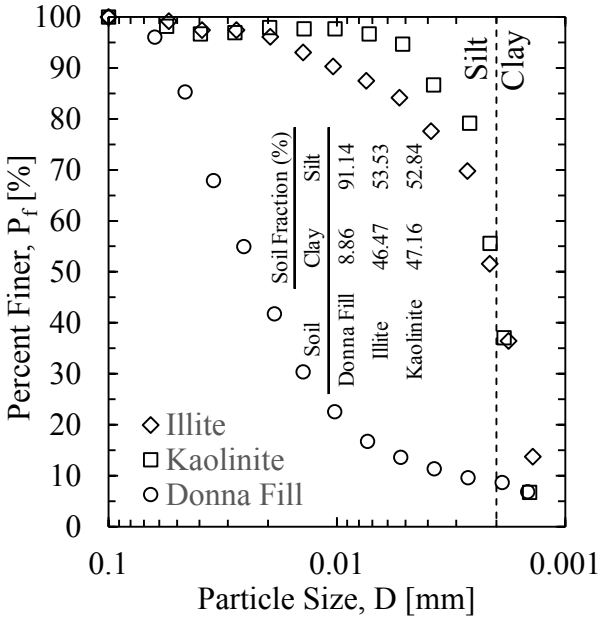

(a)

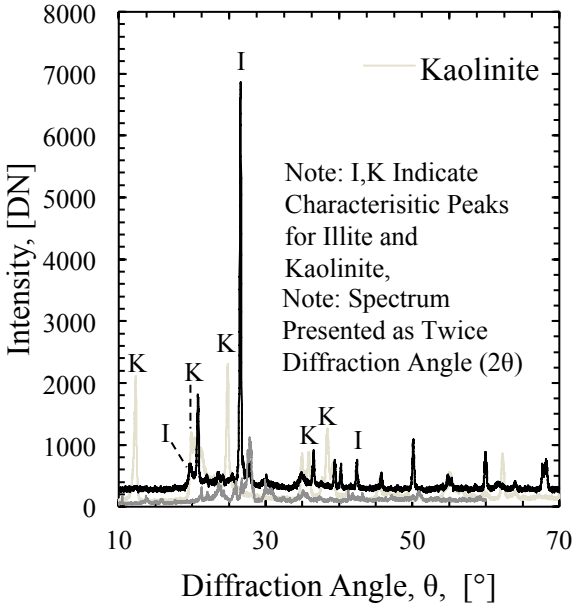

(b)

Figure 5.3. a) Soil particle distribution as determined by using ASTM D422 (2012) and b) XRD pattern for each soil type.

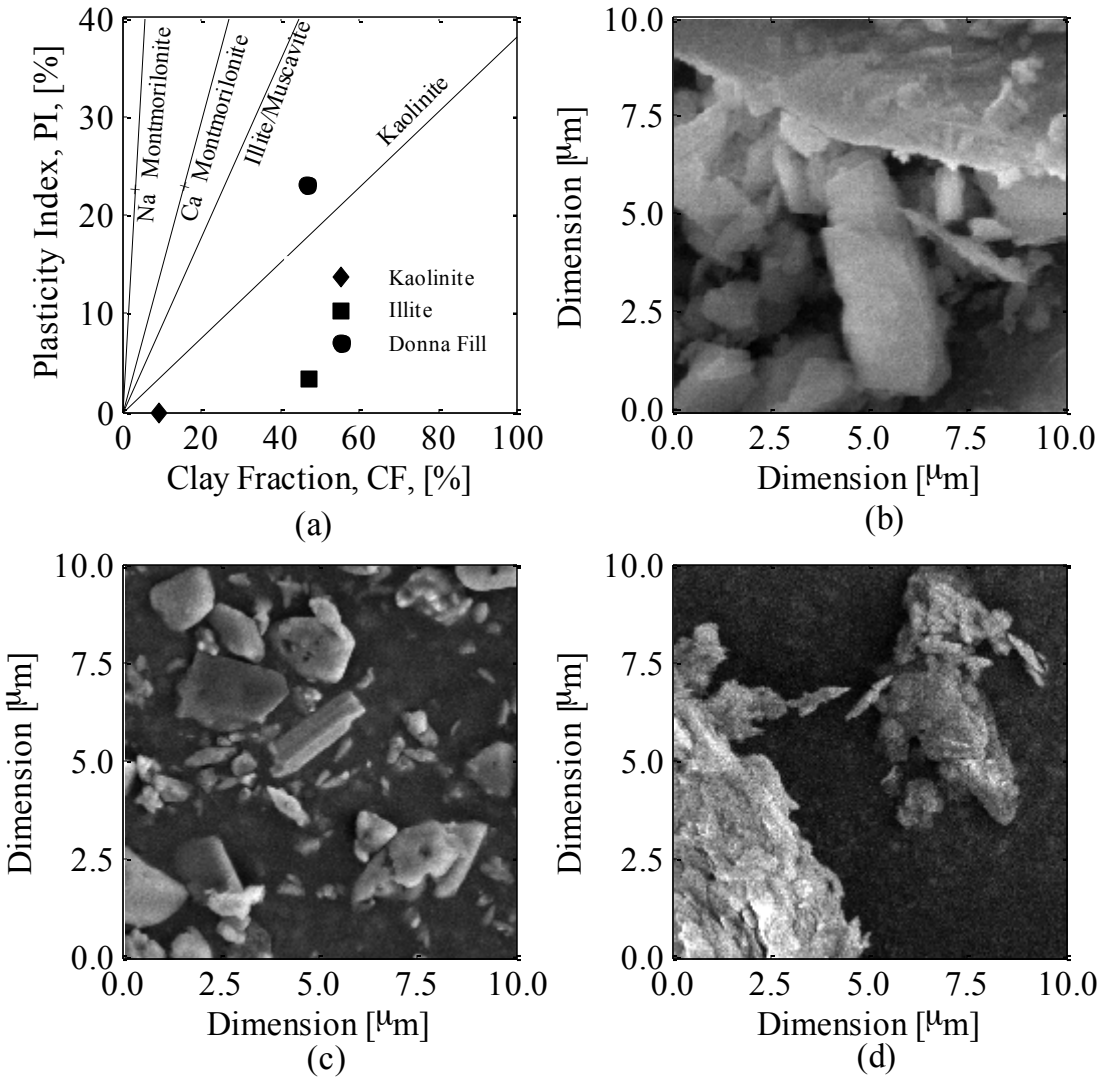

Figure 5.4. Soil mineralogy as obtained using a) traditional index testing (33) and SEM microscopy for b) Donna Fill, c) Illite, and d) Kaolinite.

5.5.2. Results from Visible to Near Infrared (400 to 2500nm) on Oven-Dried Samples (VisNIR-Dry)

The K-fold cross-validation testing on the calibration data set for the LL-, PL, and CF-PLS models, had a lower values of EMSPE at each value of N_c than the LL-, PL-, and CF-PCR models. Furthermore, the PLS regression typically required a smaller N_c value to explain greater than 95 percent of the variability in **Y**. While the EMSPE for the PL-PLS model indicated that a N_c value of two was sufficient to provide an accurate prediction, and an N_c value of three was sufficient for the CF model, the first four components were used in the model for consistency. For all the LL and CF empirical models, an N_c value of four was chosen for the PLS model (Figure 5.5). The normalized

predicted results of the three index properties (predicted values) as a function of the normalized measured values are presented as Figure 5.5.

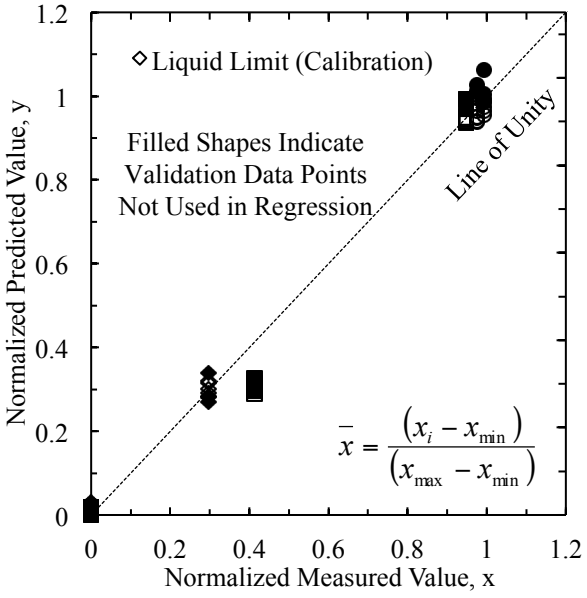

(a)

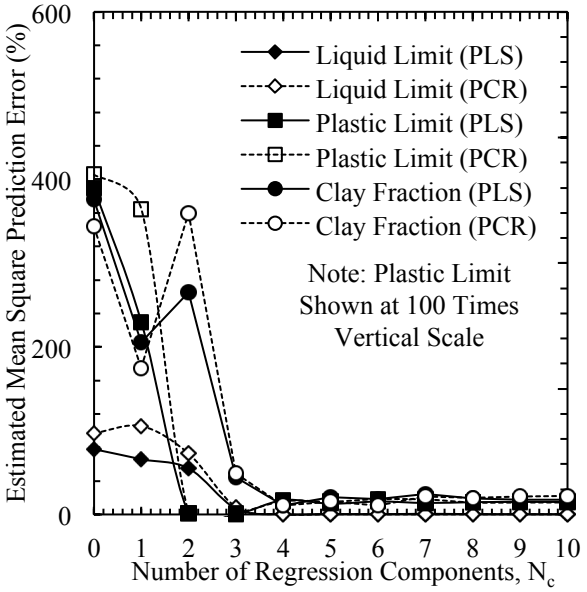

(b)

Figure 5.5. a) Normalized predicted values versus normalized measured values and b) estimated mean square prediction error as a function of number of regression components using cross validation as obtained from PLS regression on VisNIR-Dry spectrum for liquid limit, plastic limit, and clay fraction.

For all three empirical models (LL, PL, and CF) R^2 values of 0.999 were obtained. A negative bias value of -0.06 percent water content, 0.00 percent water content

and a positive value of 0.61 percent clay mass content ($g \cdot g^{-1}$) was determined for the LL, PL, and CF models, respectively. The computed standard deviation of the LL, PL, and CF models was 0.32 percent water content, 0.03 percent water content, and 2.86 percent clay mass content.

5.5.3. Results from Middle Infrared (2500 to 25000nm) on Oven Dried Samples

From the K-fold cross-validation testing on the calibration data set, the PLS regression had a lower value of EMSPE for each value of N_c than the PCR regression. Furthermore, the PLS regression typically required a smaller N_c value to explain greater than 95 percent of the variability in **Y**. The normalized values for the predicted results of the three index properties (predicted values) versus the normalized measured values are presented in Figure 5.6.

For all three empirical models (LL, PL, and CF) an N_c value of 4 was chosen for the PLS model. The squared value of the regression coefficients (R^2) for the MIR data was 0.957, 0.931, and 0.876 for the LL, PL, and CF models, respectively. A negative bias (e.g. the predicted values were less than the observed values) of 0.66 percent water content ($g \cdot g^{-1}$), 0.05 percent water content ($g \cdot g^{-1}$), and 0.3 percent clay mass fraction was computed for the LL, PL, and CF models, respectively. However, at low values of the LL, PL, and CF (specifically the Donna Fill samples) the model had a positive bias. The computed standard deviation of the entire data set (cross-validation and independent validation data) was 1.22 percent water content, 0.32 percent water content, and 2.86 percent clay mass content for the LL, PL, and CF models, respectively. The aforementioned values are indicative of a strong empirical correlation between MIR spectra and the value of the plastic limit. The CF model, conversely, provided a much less precise (+/- 3 percent), but the predicted values could be employed for soil classification. The performance of the individual PLS models, to predict the soil values, was different from the performance reported by Waruru et al. (14). Waruru et al. (14) reported values for African soils for which the statistical regression provided the best performance for measurement of LL (not PL) and the worst performance for measurement of CF.

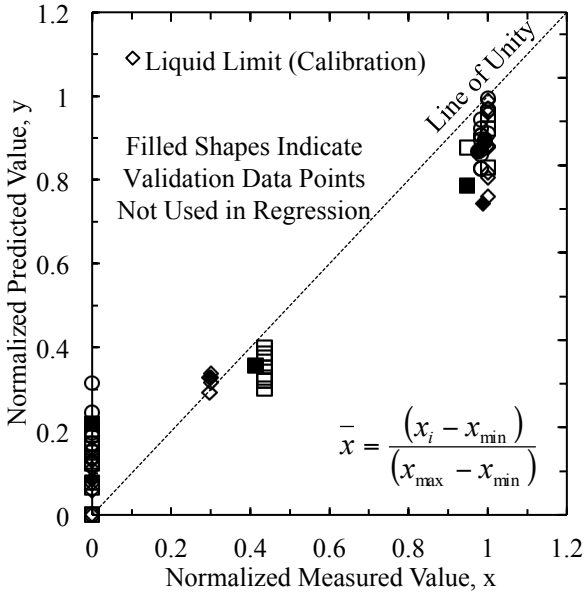

(a)

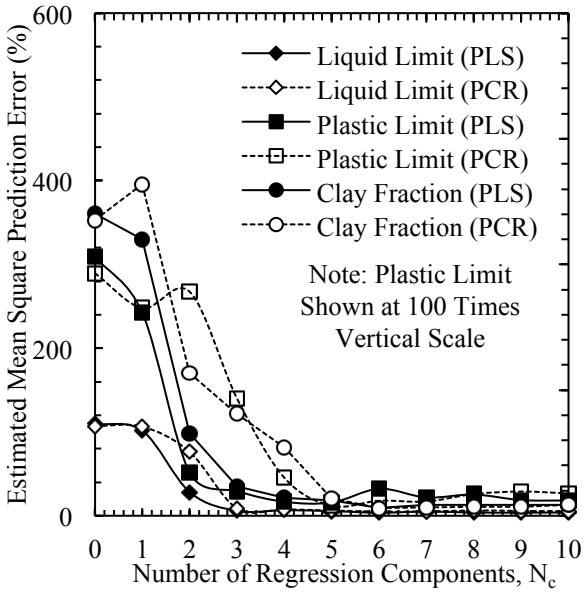

(b)

Figure 5.6 a) Normalized predicted values versus normalized measured values and b) estimated mean square prediction error as a function of number of regression components using cross validation as obtained from PLS regression on MIR spectrum for liquid limit, plastic limit, and clay fraction.

5.5.4. Results from Visible to Near Infrared (400 to 2500nm) on Intact Wet Samples (VisNIR-Wet)

As expected, due to the influence of soil water, the empirical correlation between the observed VisNIR reflectance spectrum and the measured LL, PL, and CF models were not as precise as the empirical correlations on the oven dry ground samples. A PLS model with four component ($N_c = 4$) provided EMSPE values near the minimum values encountered for the LL and PL models. For the CF model, however, the computed value of EMSPE was decreased as the value of N_c approached 10 (Figure 5.7).

Regression Coefficient (R^2) values of 0.777, 0.909, and 0.589 were calculated for the LL, PL, and CF models. However, as previously mentioned, increasing the N_c value to 10 for the CF model increased the R^2 value to 0.875 for the calibration set. The LL PLS model index value had a negative bias of 0.22 percent water content and a standard deviation of 2.44 percent water content. The value of the positive bias decreased with increasing values of LL. The PL PLS model had a positive bias of 0.61 and a standard deviation of 0.04 percent water content. Similarly, the CF PLS model had a positive bias of 0.22 percent clay and a standard deviation of 5.12 percent clay.

5.5.5. Comparison of the Three Reflectance Methods (MIR-Dry, VisNIR-Dry, and VisNIR-Wet)

For all three methods, the empirical correlation between PL and the observed reflectance data provided the lowest value of standard deviation and highest R^2 values. Similarly, the least precise method (highest standard deviation) and lowest value of R^2 was computed for empirical correlations between values of soil CF and the observed reflectance spectra. The VisNIR-Dry and MIR-Dry empirical correlations provided similar results for the three soils investigated. The results obtained from the cross-validation of the PLS models are presented in a tabular form as Table 5.1. The value of the computed VisNIR-Dry regression coefficient (R^2) was numerically larger than the values calculated for the MIR-Dry empirical correlation (0.999, 0.999, and 0.999 versus 0.957, 0.931, and 0.876, for LL, PL, and CF, respectively). In addition, the empirical relationships between the VisNIR-Dry had a lower standard deviation for all three PLS models relative to the empirical correlation obtained from the MIR-Dry spectra (0.32, 0.04, and 0.61 percent versus 1.22, 0.31, and 2.86 percent). The standard deviation for the LL methods obtained with VisNIR-Dry and MIR-Dry were smaller than or equivalent to the acceptable standard deviation (1.3 percent for ML soils) for the traditional laboratory testing techniques, as reported in (1). The VisNIR-Dry and MIR-Dry PL PLS models had predicted standard deviation values that were comparable to the acceptable value of standard deviation of 1.2 percentage points as reported in (1). In particular, the PL relationships obtained for the VisNIR-Dry, MIR-Dry, and VisNIR-Wet techniques had a coefficient of variability value (1.0 percent, 0.1 percent, and 2.5 percent, respectively) that was below the variability value reported Waruru et al. (14) for traditional plastic limit testing (9.2 percent).

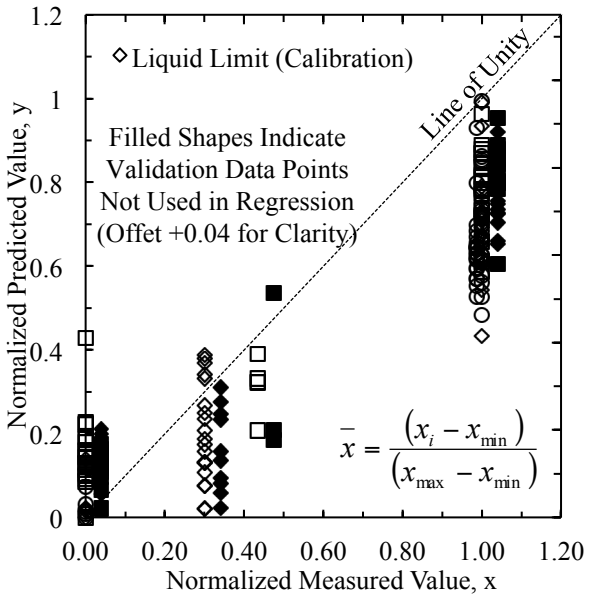

(a)

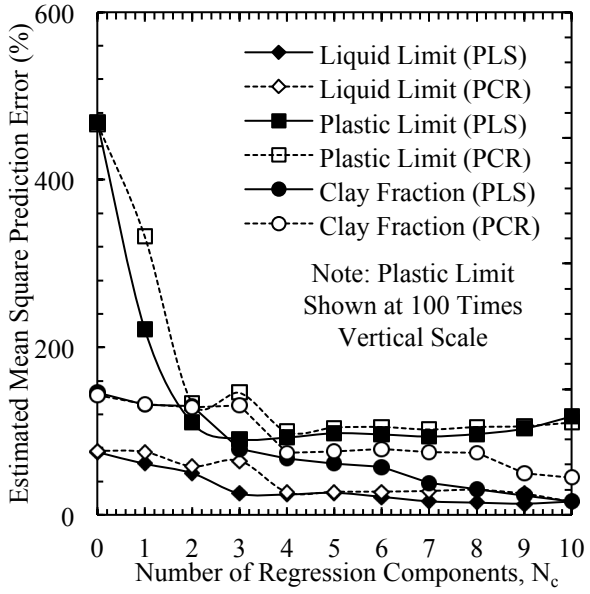

(b)

Figure 5.7. a) Normalized predicted values versus normalized measured values and b) estimated mean square prediction error as a function of number of regression components using cross validation as obtained from PLS regression on VisNIR-West spectrum for liquid limit, plastic limit, and clay fraction.

Table 5.1. Minimum, Maximum, Mean, Bias, and Standard Deviation of PLS Models for LL, PL, and CF for MIR-Dry, VisNIR-Dry, and VisNIR-Wet

Method	Property	Material	All Values as Percentage					
			Measured	Min	Max	Mean	Bias	Standard Deviation
MIR-Dry								
MIR-Dry	LL	Kaolinite	31.5	30.66	31.88	31.41	0.09	0.42
MIR-Dry	LL	Illite	46.7	42.72	49.36	46.08	2.21	2.04
MIR-Dry	LL	Donna Fill	25	22.84	27.1	25.32	-0.32	1.2
VisNIR-Dry	**LL**	**Kaolinite**	**31.5**	**30.82**	**32.35**	**31.47**	**0.03**	**0.48**
VisNIR-Dry	**LL**	**Illite**	**46.7**	**46.61**	**47.18**	**46.86**	**-0.16**	**0.22**
VisNIR-Dry	**LL**	**Donna Fill**	**25**	**24.79**	**25.49**	**25.04**	**-0.04**	**0.25**
VisNir-Wet	LL	Kaolinite	31.5	25.56	36.15	31	0.5	2.83
VisNir-Wet	LL	Illite	46.7	37.25	50.97	44.24	2.46	2.5
VisNir-Wet	LL	Donna Fill	25	26.6	31.75	28.62	-3.62	1.98
VisNIR-Dry								
MIR-Dry	PL	Kaolinite	28.1	27.22	28.32	27.84	0.26	0.39
MIR-Dry	PL	Illite	23.6	23.09	24.23	23.7	-0.1	0.38
MIR-Dry	PL	Donna Fill	25	24.75	25.29	25	0	0.17
VisNIR-Dry	**PL**	**Kaolinite**	**28.1**	**26.07**	**25.15**	**28.11**	**-0.01**	**0.03**
VisNIR-Dry	**PL**	**Illite**	**23.6**	**23.56**	**23.65**	**23.6**	**0**	**0.04**
VisNIR-Dry	**PL**	**Donna Fill**	**25**	**24.94**	**25.07**	**25**	**0**	**0.04**
VisNir-Wet	PL	Kaolinite	28.1	26.06	28.48	27.48	0.62	0.61
VisNir-Wet	PL	Illite	23.6	22.13	25.05	23.11	0.49	0.5
VisNir-Wet	PL	Donna Fill	25	23.78	26.11	24.68	0.32	0.73
VisNIR-Wet								
MIR-Dry	CF	Kaolinite	47.16	43.65	50.69	47.19	-0.03	2.54
MIR-Dry	CF	Illite	46.47	42.29	48.12	44.9	1.57	1.97
MIR-Dry	CF	Donna Fill	8.9	1.07	16.81	9.55	-0.65	4.08
VisNIR-Dry	**CF**	**Kaolinite**	**47.16**	**46.09**	**48.95**	**47.22**	**-0.06**	**0.87**
VisNIR-Dry	**CF**	**Illite**	**46.47**	**45.79**	**47.6**	**46.55**	**-0.08**	**0.58**
VisNIR-Dry	**CF**	**Donna Fill**	**8.9**	**8.66**	**9.62**	**9.02**	**-0.12**	**0.39**
VisNir-Wet	CF	Kaolinite	47.16	32.14	64.46	45.65	1.51	7.3
VisNir-Wet	CF	Illite	46.47	37.92	61.27	44.91	1.56	4.33
VisNir-Wet	CF	Donna Fill	8.9	7.37	16.56	11.3	-2.4	3.74

Bold Text Indicates the Remote Sensing Test with the Lowest Standard Deviation

The degradation of the performance of the empirical correlation between the VisNIR-Dry and VisNIR-Wet samples is hypothesized to be primarily caused by the strong influence of water within specific wavelength ranges. Values of soil water content have been reported to be strongly influence the soil reflectance spectrum within in the visible portion of the spectrum as well as within absorption feature between 1800 and 2100 nm (27). This wavelength range corresponds to high absolute values of weighting coefficients (indicating a strong correlation between data in this wavelength range and the

measured values of LL and CF) for the 1st and 4th PLS components in the LL VisNIR-Dry correlation and the 1st, 3rd, and 4th components of the CF VisNIR-Dry correlations. Conversely, for the LL and CF VisNIR-Wet correlations, low absolute values of weighting coefficients between approximately 1800 and 2200 nm were observed for the 1st, 3rd, and 4th PLS components in LL model and for the 1st, 2nd, 3rd, and 4th PLS components in the CF model. It is possible that the model performance may be improved by the use of additional soil spectra (and particularly from additional soil types) and a larger calibration and validation data set. Additionally, although not investigated as part of this work, other researchers have proposed using additional data transformations (e.g. using the first and second derivatives of the reflectance spectra instead of the raw reflectance spectra) prior to performing the statistical regression.

5.6. Recommendations and Conclusions

VisNIR spectroscopy has several potential benefits relative to the existing standard of practice for obtaining soil index properties. Specifically, VisNIR spectroscopy is rapid (spectrum acquisition in minutes), repeatable (4), and has the potential to be non-destructive (e.g. VisNIR-Wet). The variability of the remotely sensed measurements of soil LL were similar to the variability reported in ASTM D4318 (1). However, for measurements of the PL, the results of this investigation indicated a higher precision than the existing standard of practice (1). The use of oven-dried ground soils does provide an increased correlation value (R^2) and reduced standard deviation for all measurements of LL, PL, and CF. Specifically, the lowest variability and bias in the remotely sensed measurements were observed in in the VisNIR-Dry samples. However, the use of oven-dried samples does negate the non-destructive, rapid testing benefits of the remotely sensed technology. However, even with oven-dried samples, VisNIR spectroscopy is less time consuming than the traditional testing methods.

Based on the obtained results, another potential application for this technology may be as an initial characterization technique to identify soils of greatest interest to engineering professionals. For example in a transportation or geo-environmental application where the index properties (LL, PL, and CF) partially control the selection of suitable borrow material, a properly calibrated (site-specific) remote sensing instrument could be used to identify locations of suitable materials. Similarly, such an instrument could be utilized in a quality control and assurance program to rapidly assess material prior to and during placement (similar to the function of the nuclear density gauge for in-situ density measurements).

Acknowledgements: This work was in part sponsored by the United States Department of Transportation Office of the Assistant Secretary for Research and Technology (USDOT/OST-R) under grant number ASRTRS-14-H-UARK: Remote Sensing Based Assessment System for Evaluating Risk to Transportation Infrastructure Following Wildfires. The authors would like to express their gratitude to the USDOT/OST-R. The views, opinions, findings, and conclusions reflected in this manuscript are the responsibility of the authors only and do not represent the official policy or position of the USDOT/OST-R, or any state or other entity.

Chapter 6: Development of a Ground-based Remote Sensing Device

The use of satellite-, and ground-based thermal, radar, and lidar technologies was proposed to enable acquisition of specific parameters of interest to characterize the risk of mudflows or rockslides at a specific site. The NASA Soil Moisture Active Passive (SMAP) satellite sensor, that was to be used for this project, malfunctioned. Instead only LANDSAT imagery was used for the decision support model (as described in Chapters 2 and 3). The proposed ground-based remote sensing device was developed and utilized for this project. As proposed, the soil observation differential absorption lidar (SOTDiAL), ground-based data were obtained from: a modified version of the existing University of Arkansas Gamma Remote Sensing portable radar interferometer version II (GPRI-II), a topographic differential absorption light detection and ranging (TDiAL) module, and the directional gamma-ray spectrometer (DiGS) module. Photographs of the current versions of the GPRI-II and TDiAL modules of the ground-based device, in use at the location of the Soda Fire in Idaho, are presented in Figures 6.1.

(a) (b)

Figure 6.1. Photographs of the a) newly created TDiAL and b) modified GPRI-II at the location of the Soda Fire in Idaho.

The majority of near-surface (i.e. above the water table) soil mechanics are governed by soils that are in an unsaturated (partially saturated) condition. Unsaturated soil behavior (e.g. shear strength, permeability) is controlled by parameters of the soil including volumetric water content, soil matric potential (suction), and clay mineralogy. The geotechnical engineering community has recognized the importance of unsaturated

soil behavior and therefore efforts to account for and to model unsaturated soil behavior are becoming increasingly prevalent in engineering design.

The ability to infer and quantify saturated and unsaturated soil properties using a remote sensor has the potential to improve the current state of the practice of data collection. The remote sensing techniques that were used for this project will allow for the rapid collection of spatially vast data as compared with traditional, spatially limited in-situ or laboratory methods, which rely on 1) individually calibrated instruments installed into the ground (e.g. tensiometers), or 2) samples recovered from the field and tested in the laboratory setting (e.g. dewpoint potentiometer). With the equipment described in this chapter, data may be collected from afar and on-demand from a single vantage point, all of which improve site accessibility and collection efficiency. Despite the initial buy-in costs, savings may be realized over time through the low cost-per-area application of the remote sensing technique. The disadvantage of collecting these measurements remotely is the limitation on penetration depth. All measurements are acquired from the surface of the soil and measurement values beneath the surface must be estimated through correlations to the surface measurement. Furthermore, like many other types of remote sensing techniques, vegetative cover on the soil will not allow for accurate measurement of the soil properties. The techniques that were used for this project are therefore best suited to bare soil surfaces, like those found after wildland fires.

The applications for the developed remote sensor extend beyond the immediate scope of geotechnical engineering. The technology may ultimately be applied to hydrological studies, agricultural science, and forensic investigation of geohazards (landslides, debris flows, etc.). The technology could also be applied to the rapid assessment of soil faces or tailings for mining operations. The proposed adaptation of diffuse reflectance spectroscopy and the DIAL technique to infer soil properties from a remote platform is novel and therefore, there may be other future applications.

The SOTDIAL instrument was designed and assembled utilizing almost entirely commercial-off-the-shelf (COTS) parts. Although this may have increased the total cost of the instrument, it eliminated the need for in-house, custom part fabrication (e.g. external cavity laser diode). The use of COTS parts was an attractive attribute of the instrument because the same parts are available to other research programs that wish to adapt the design of the instrument.

The SOTDiAL instrument was developed in five phases. *1)* Component design (transmitter, receiver, data acquisition and control) and compilation of a parts list. *2)* Acquisition and testing of the major components. *3)* Assembly and preliminary testing of each instrument component. *4)* Testing of the instrument in the laboratory setting. *5)* Field ruggedization of the instrument. The details of the SOTDIAL instrument development are further described in Section 6.1. An outline of testing and validation of the technique are described in Section 6.2.

6.1. Instrument Design

The SOTDiAL instrument combined three technologies: traditional lidar altimetry, DiAL (active detection), and reflectance spectroscopy (active and passive detection). The SOTDiAL instrument was comprised of *1)* an active laser delivery and transmitting system, *2)* a dual-channel receiving system (active and passive measurements), and *3)* a data acquisition and control system (RF signal processing and component control). The ranging portion of the instrument (transmitter and receiver) was designed using a self-chirped coherent homodyne detection scheme that was similar to the system described by Adany et al. (2009). The DiAL portion of the instrument (transmitter and receiver) was seeded by an amplitude-modulated (AM) continuous-wave (CW) laser with the ability to switch between on-line and off-line wavelengths. The reflectance spectroscopy portion of the instrument (receiver only) allows for the collection of additional data and also allows for verification of data collected by the altimeter and DiAL portions of the instrument.

6.1.1. Transmitter

To aid in the appropriate delivery of two distinct laser wavelengths, through the transmitter along the same transmitter-receiver path, the transmitter system was constructed as partially free-space based and partially fiber-optic based. The optical carrier signal was seeded by two precision tunable external cavity diode lasers (ECDL), which produce continuous waveform (CW), low power outputs (approx. 17 mW at usual operating currents) at stable wavelengths of 823.20 nm and 847.00 nm with narrow linewidths $\leq$ 200 kHz. Both ECDL were powered with separate controllers; the data acquisition system will eliminate the need for external function generation while reducing noise. The ECDL were coupled in free space using narrowband polarization-dependent Faraday isolators. A series of dielectric mirrors directs each laser beam into a polarization-maintaining (PM) fiber optic cable via an aspheric collimation coupler. Optomechanical shutters were also installed in the laser paths to provide a fail-safe. These shutters are controlled remotely. The light energy within the fiber optic cable was then coupled into a Mach-Zehnder electro-optic intensity modulator (MZM) where the amplitude of the incoming light was modulated. The modulation of the transmitted light was necessary to identify backscattered light through the receiver. The modulation was achieved by utilizing a high frequency RF signal generator to encode the transmitted light with a linear chirp (large bandwidth ramping signal).

After modulation, the light was split using an optical beamsplitting cube. Seventy (70) percent of the energy continued along the transmitter path and the remaining 30 percent of the energy was redirected to the balanced photodetector (BPD) to act as the local oscillator (LO) for the simplified homodyne altimeter portion of the system. The light that traveled along the transmitter path was amplified through a tapered semiconductor optical amplifier (TSOA) before being transmitted out of the system and into the atmosphere through a variable beam expander. A schematic of the SOTDiAL is presented in Figure 6.2.

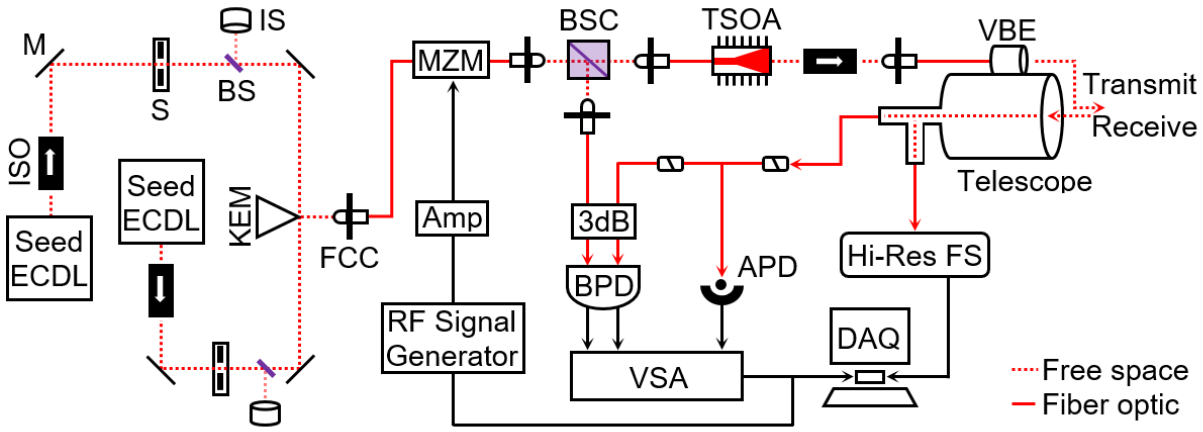

ECDL = External cavity diode laser; ISO = Optical isolator; M = Dielectric mirror;
S = Shutter; BS = Beam sampler; IS = Integrating sphere; KEM = Knife-edge mirror;
FCC = Fiberport collimation coupler; MZM = Mach-Zehnder-amplitude modulator;
BSC = Beamsplitter cube; TSOA = Tapered semiconductor optical amplifier;
VBE = Variable beam expander; Hi-Res FS = High-resolution field spectroradiometer;
APD = Avalanche photodetector; BPD = Balanced photodetector; VSA = Vector signal analyzer

Figure. 6.2. Schematic of the major parts of the SOTDiAL instrument.

6.1.2. Receiver

The receiver system was comprised of ranging altimeter, DiAL, and passive detection components. The design of the DiAL components of the receiver was based on optical receivers currently in operation for other DiAL instruments (Repasky 2016). The main aperture of the receiver collects light for all three components with an 8-in. diameter, f/10 catadioptric Schmidt-Cassegrain telescope. Light is then successively collimated and focused through a series of coated and uncoated lenses contained within an enclosed dual-channel optical receiver assembly that is attached to the back of the telescope. An adjustable iris is located behind the telescope, within the optical receiver assembly, to act as the field stop for the receiver. The lens designs was calculated using the equation for focal length of a thick lens, presented as Equation 6.1, and a Gaussian beam shaping equation, presented as Equation 6.2.

$$\frac{1}{f} = (n-1)\cdot\left(\frac{1}{r_1} - \frac{1}{r_2}\right) + \left(\frac{d\cdot(n-1)^2}{n\cdot r_1\cdot r_2}\right) \qquad \text{(Jenkins and White 1937)} \qquad \text{[Eq. 6.1]}$$

$$r_c = (r_t)\cdot\frac{f_c}{f_t} \qquad \text{(Repasky 2016)} \qquad \text{[Eq. 6.2]}$$

In Equation 6.1, f is the effective focal length for a thick lens, n is the index of refraction of the lens material, r_1 and r_2 are the lens surface radii, and d is the lens thickness. In Equation 6.2, r_c and r_t are the aperture radii of the collimating lens and the telescope, respectively, and f_c and f_t are the focal lengths of the collimating lens and the telescope, respectively.

The light was split using an uncoated 50:50 beamsplitter; the light was then focused into *1)* optical fiber passing to a high resolution spectroradiometer instrument (ASD FieldSpec 4 Hi-Res) and *2)* optical fiber passing to the ranging and DiAL portions of the SOTDiAL system. To couple the incoming free-space light beams with the optical fibers efficiently, the acceptance angles for the optical fibers were calculated using Equations 6.3 through 6.5. The full-angle-field-of-view (FOV) of the instrument will be calculated using Equation 6.6.

$$\frac{f}{N} = (2 \cdot \mathrm{NA_t})^{-1} \quad \text{(Allen et al. 2001)} \quad \text{[Eq. 6.3]}$$

$$\theta_a = \sin^{-1}(\mathrm{NA_f}) \quad \text{(Repasky 2016)} \quad \text{[Eq. 6.4]}$$

$$\frac{\mathrm{D}}{\mathrm{f_{FP}}} = \mathrm{NA_f} \quad \text{(Repasky 2016)} \quad \text{[Eq. 6.5]}$$

$$\mathrm{FOV} = \frac{2 \cdot \mathrm{R}}{\mathrm{f_t}} \quad \text{(Repasky 2016)} \quad \text{[Eq. 6.6]}$$

In Equation 6.3, $\frac{f}{N}$ is the focal ratio of the telescope (N is the f-number), NA_t is the nominal aperture of the telescope. In Equation 6.4, θ_a is the acceptance angle of the optical fiber in radians, NA_f is the nominal aperture of the optical fiber. In Equation 6.5, D is the diameter of light incident on the fiberport collimator, f_{FP} is the focal length of the fiberport collimator. In Equation 6.6, R is the beam radius of the incoming light, and f_t is the focal length of the telescope.

For the spectroradiometer, the light collected through the telescope remains unfiltered. However, for the ranging and DIAL receivers, where only the detection of the backscattered, actively transmitted, wavelengths (823.20 and 847.00 nm) is desired, the amount of background light was reduced using two interchangeable narrow bandpass filters (NBF). A schematic of the design of the dual-channel optical receiver is presented in Figure 6.3. The light transmitted through the multimode fiber was split through a series of fiber optic couplers to divert light *1)* into the BPD to measure the beat frequency (for range measurements) and *2)* into an avalanche photodetector (APD) to measure frequency for range-resolved detection of water vapor in the atmosphere (for DiAL measurements).

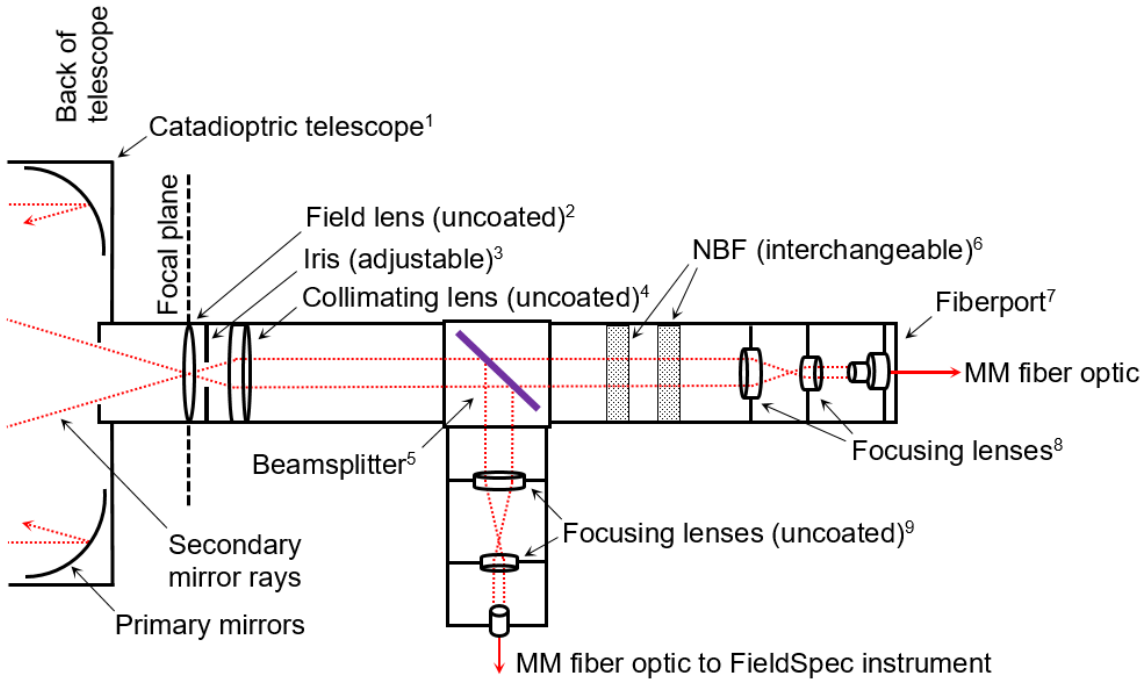

[1]Field aperture, Ø = 203.2mm, f/10, *f* = 2003mm; [2]Uncoated N-BK7 biconvex lens, *f* = 50mm; [3]Manually adjustable iris diaphragm; [4]Uncoated N-BK7 spherical lens, *f* = 50mm; [5]Uncoated broad transmission, 50/50 polka-dot beamsplitter; [6]Narrow bandpass filters; [7]NIR-coated fiberport, *f* = 4.6mm; [8]NIR-coated achromatic doublets, *f* = 25mm, *f* = 10mm; [9]Uncoated aspheric lenses, *f* = 12mm, *f* = 8mm

Figure. 6.3. Dual-channel optical receiver design for proposed SOTDiAL instrument.

6.1.3. Data Acquisition System

The data from the BPD and APD were collected with a 6.6-GHz Vector Signal Analyzer (VSA) mounted in a data acquisition and control chassis (National Instruments). The data were interpreted by an onboard, chassis-mounted computer in a Windows operating environment. Furthermore, individual components within the SOTDIAL system were controlled by National Instruments cards mounted in the chassis (RF signal generation for electro-optic light modulation within the MZM, voltage/current supply for electromechanical shutters, laser power control and feedback metrics). The BPD, APD, TSOA (and TSOA thermo-electric mount) were each powered and self-regulated with external controllers that may be easily accessed alongside the data acquisition and control chassis.

6.2. Testing and Validation

6.2.1. Instrument Testing

The testing of the SOTDiAL instrument was completed in the following stages. The first stage included testing the transmission light quality (power and polarization) at the source (ECDL), before and after signal modulation through the MZM, before and after splitting occurs through the beamsplitting cube, and before and after amplification

through the TSOA. Additionally, the RF signal generator (for the MZM) and the TSOA controllers were tested to ensure that the expected performance characteristics were achieved (signal quality, temperature stability). The second stage of testing included testing the dual-channel optical receiver, testing of each of the photodetectors (BPD and APD), and testing the data acquisition system. The third stage of testing utilized the fully-assembled SOTDiAL instrument to test the range measurement, the DIAL measurement, and the spectroradiometry measurement capabilities (within the laboratory). The fourth stage of testing involved field testing of the ruggedized instrument. The overlap profile of the SOTDiAL system wasdetermined according to the procedures outlined in Hey et al. (2011). Data from each stage of testing were analyzed and compiled for future reference.

6.2.2. Validation

The Garner (2017) methodology was utilized to validate the measurements collected with the SOTDiAL instrument. Both empirical and analytical solutions were attempted. The laboratory measurements followed the Garner (2017) DRIFT and LAST techniques. Laboratory measurements from the SOTDiAL instrument were compared with measurements from laboratory testing of centrifuge prepared soil specimens with known characteristics (water content, soil suction, plasticity, clay content). Field measurements included range-resolved measurements of backscatter from 1) hard targets (soil at ground surface) and from 2) differential absorption to account for the amount of atmospheric moisture encountered en route to the soil surface. The inferred measurements were compared with measurements collected using traditional in-situ instrumentation (tensiometer) and samples recovered from the field and tested in the laboratory (dewpoint potentiometer, sieve analysis, Atterberg limit tests).

Results obtained during the development of the SOTDiAL will be included in archival journal articles. Sean Salazar will write these articles as part of his doctoral dissertation, under the guidance of Richard Coffman. The articles will be written and submitted to the respective journals before Sean defends his dissertation in May of 2019. Although the journals may be submitted to may change, the titles of the articles and the proposed journals are described in this section. The development of the SOTDiAL instrument will be outlined in a publication, entitled “Development of a Multimode Field Deployable Lidar Instrument for Measurement of Unsaturated Soil Properties” that will be submitted to *Remote Sensing of Environment*. The publication will include the specific details of the design and characteristics of the instrument. A follow-up publication will focus on the optical design and testing of the dual-channel instrument receiver in an article entitled “Dual-Channel Optical Receiver for Ground-Based Topographic DiAL Sensing”, submitted to *Optical Engineering*. A third journal publication will also be prepared. This article will be submitted to *Remote Sensing of Environment*, and will be entitled “Unsaturated Soil Measurements from a Topographic DiAL Instrument.” The results from the laboratory and field tests of the SOTDiAL instrument will be presented in this publication. A user manual was also prepared for the SOTDiAL instrument and was made available to future operators and researchers. In addition to the aforementioned journal articles, the patent application that was filed for the SOTDiAL is also included as Appendix F, for completeness.

Chapter 7: Conclusions, Outcomes, and Deliverables

A remote sensing-based system for evaluating hazard to transportation infrastructure, following wildfire events, was developed in a two-phase research project. One phase focused on the advancement of predictive, GIS-based, post-wildfire debris flow modeling techniques, while the other phase focused on the development of novel remote sensing instrumentation and techniques for collecting data associated with the debris flows. The focus of the debris flow modeling phase was to significantly improve the prediction capability of existing models by evaluating 1) the sensitivity to remotely-sensed input data and 2) the probabilistic algorithms used to predict debris flow occurrence. A rapid, web-based delivery system was instituted to provide a debris flow prediction mapping service to requesting agencies. The maps were hosted within the interactive, web-based NASA Rehabilitation Capability Convergence for Ecosystem Recovery (RECOVER) platform for ease of access. Quantification of the potential impact to transportation infrastructure, primarily roadways, was also evaluated as part of the project (Figure 7.1). The significance of this phase was the marked improvement to the state-of-the-art of debris flow modeling.

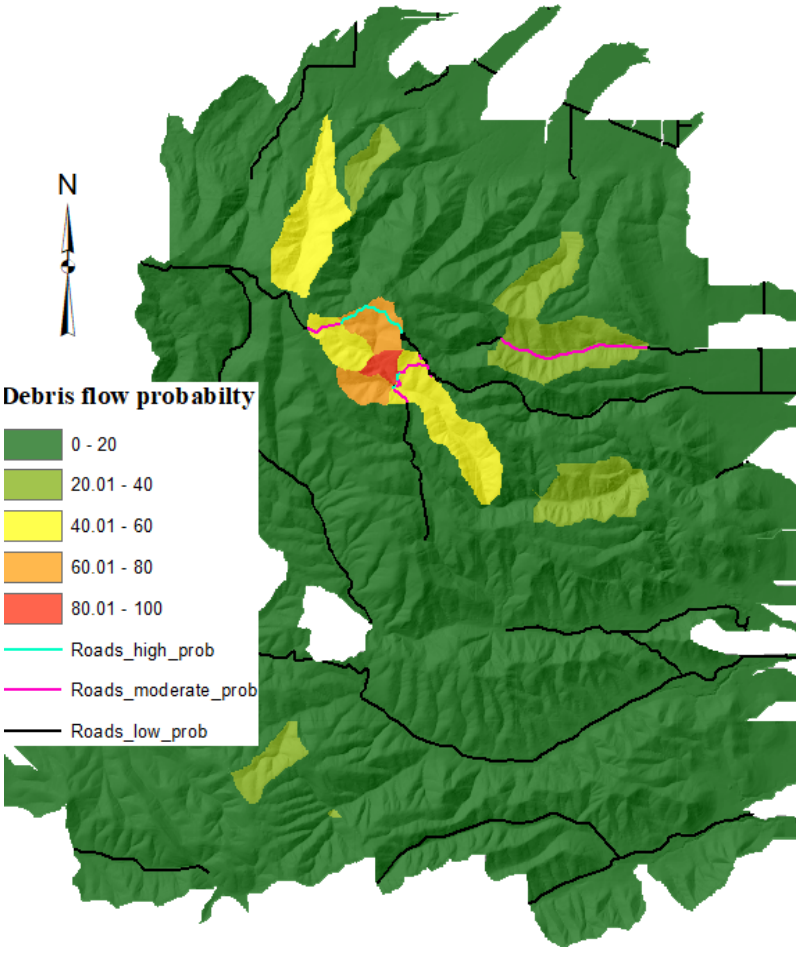

Figure 7.1. Example of a debris flow probability map, indicating hazard to transportation infrastructure (Stateline Fire, Utah-Idaho border, 2013).

The focus of the instrument development phase was the application of remote sensing techniques to the collection of input data for modeling, primarily saturated and unsaturated soil parameters. The significance of this phase was the development of emerging and novel remote sensing techniques. Both phases of the project were successfully implemented and the research results were disseminated through various conference presentations, journal article publications, and stakeholder workshops.

7.1. Significant Findings and Outputs

Machine learning-based probability models for predicting post-wildfire debris flows within the fire perimeter were developed. These models were trained and validated on datasets across the intermountain and western United States regions. The models improved on the prediction ability over current, commonly accepted, linear regression models in the literature by almost a factor of two.

The predictive models were hosted on the NASA RECOVER online platform in cooperation with the Idaho State University's GIS Training and Research Center. Debris flow hazard web map requests were fulfilled for over 20 wildfire sites in 6 states. The maps were typically delivered to the requesting agency within a day. This alone provided a valuable improvement in service over previous model delivery schedules, which were typically on the order of weeks.

The input parameters for modeling were evaluated and the sensitivity to specific remotely-sensed datasets was assessed. Previously unreported relationships between already available input data, including soil parameters, were discovered. Various, new, non-linear modeling approaches were evaluated and compared to determine the most appropriate method for modeling debris flows. The findings, including the development of the probability models, were described in detail in a reputed, peer-reviewed journal publication.

In addition to predictive models for the probability of debris flows, predictive models for the volume of debris flows were developed. Like the probability models, the volume models quantified the potential erosion that will occur in the event of a debris flow within individual catchments and sub-catchments. A manuscript describing the predictive volume model is currently in preparation for publication.

Three terrestrial remote sensing techniques were developed, including a Ku-band advanced polarimetric radar interferometry technique, a gamma-ray spectroradiometry technique, and a field deployable Soil Observation Topographic Differential Absorption Lidar (SOTDIAL) technique. These three technologies demonstrated the potential improvements that could be gained over traditional methods (laboratory-based, in situ) of obtaining post-wildfire site assessment characteristics, such as vegetation indices, burn severity, and saturated and unsaturated soil parameters.

A provisional patent, and subsequent full patent application, were filed with the U.S. Patent and Trademark Office on behalf of the SOTDiAL instrument that was developed as part of this project. Efforts to commercialize this technology have ensued.
A User Manual for Terrestrial Remote Sensing techniques developed under this project was prepared and published on the project website.

7.2. Products and Outcomes

The research results have been presented at several national conferences, including the Transportation Research Board (TRB), Geotechnical Frontiers, and two annual meetings of the Association of Environmental & Engineering Geologists (AEG). Project outcomes and demonstrations were also disseminated at a NASA Applied Remote Sensing Training (ARSET) workshop, a CRS&SI Technologies workshop, three technical advisory committee meetings, and a Commercial Remote Sensing End Users Workshop. One peer-reviewed article has been published in the Mathematical Geosciences journal, with another in preparation for the journal Geomorphology. One article was submitted for publication in the Transportation Research Record and another article has been submitted to Soil Science. Four more publications are currently in preparation for submission to high impact, peer-reviewed journals, including Remote Sensing, Remote Sensing of Environment, and Journal of Applied Remote Sensing. One patent application was filed. The aforementioned outcomes have resulted in dissemination to agencies including the FHWA, USGS, Caltrans, CDOT, ODOT, DOI, BLM, USFS, INL, IFG, NASA, and researchers from university systems across the country.

7.3. Post Project Initiatives

The successful completion of this project resulted in continued interest from stakeholders, particularly in the western states. A steady queue of debris flow probability map requests from land managers in the western states has indicated that there is interest in the service (Figure 7.2). Information about the project can be found at the project websites.

https://wildfire-landslide-risk-dss.uark.edu
http://giscenter.isu.edu/research/Techpg/nasa_RECOVER/index.htm.

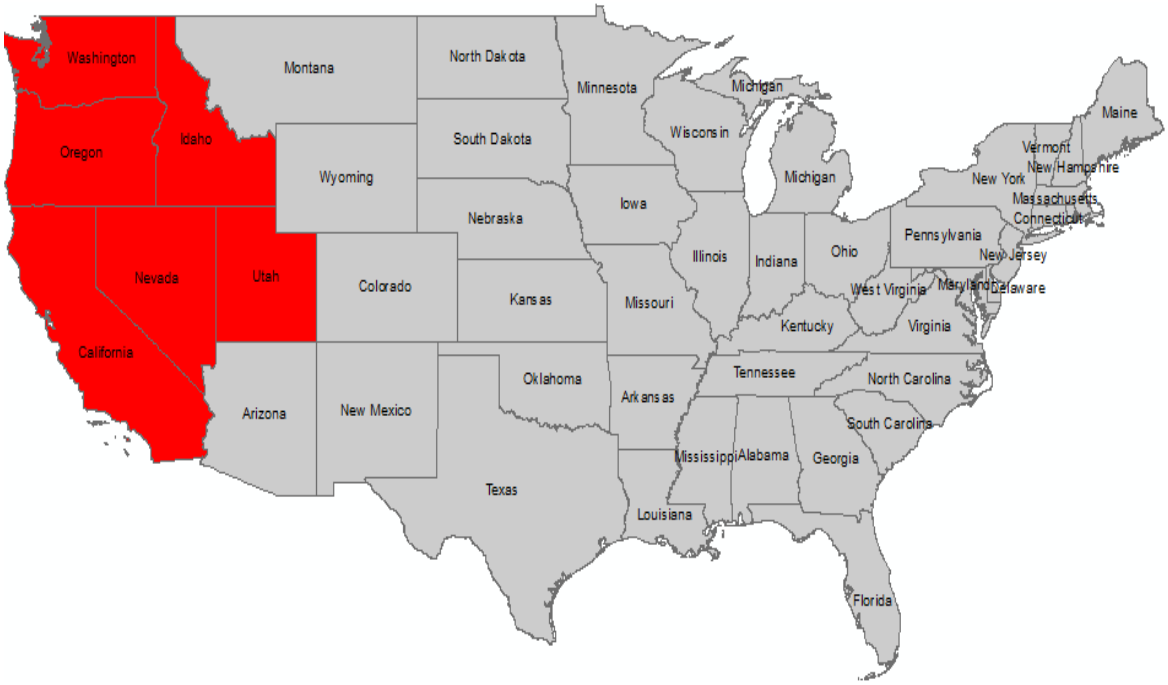

Figure 7.2. States for which debris flow mapping orders were completed.

Chapter 8: References

Adany, P., Allen, C., Hui, R., 2009, "Chirped Lidar Using Simplified Homodyne Detection," *Journal of Lightwave Technology*, Vol. 27, No. 16, pp. 3351-3357.

Allen, C., Cobanoglu, Y., Chong, S.K., Gogineni, S., 2001, "Performance of a 1319 nm Laser Radar Using RF Pulse Compression," *Proc. IGARSS,* Sydney, Australia, 2001, pp. 997-999.

American Society for Testing and Materials (ASTM), 2014, "Annual Book of Standards," American Society for Testing and Materials, Vol. 4.08, Soil and Rock (I). West Conshohocken, PA.

ASD Panalytical Inc., 2014, "RS3 and ViewSpecPro Software and Supporting Documentation," The ASD Panalytical Inc. Boulder, Colorado.

Bailey R.W., Craddock G.W., and Croft A.R., 1947, "Watershed Management for Summer Flood Control in Utah." U.S. Department of Agriculture, Forest Service, Miscellaneous Publication 639, pp. 24.

Benediktsson, J.A., Swain, P.H., and Ersoy, O.K., 1990, "Neural Network Approaches Versus Statistical-methods in Classification of Multisource Remote-sensing Data." IEEE Transactions on Geoscience and Remote Sensing, Vol. 28, No. 4, pp. 540-52. doi: 10.1109/TGRS.1990.572944.

Ben-Dor, E., Banin, A., 1995, "Near-Infrared Analysis as a Rapid Method to Simultaneously Evaluate Several Soil Properties," *Soil Science Society of America Journal*, Vol. 59, No. 2, pp. 364-372.

Bishop, A.W., Alpan, I., Blight, G.E., Donald, I.B., 1960, "Factors Controlling the Shear Strength of Partly Saturated Cohesive Soils," *Proc. ASCE Research Conference on Shear Strength of Cohesive Soils*, University of Colorado, Boulder, USA, pp. 503-532.

Blatz, J.A., Ferreira, N.J., Graham, J., 2004, "Effects of Near-Surface Environmental Conditions on Instability of an Unsaturated Soil Slope," *Canadian Geotechnical Journal*, Vol. 41, pp. 1111-1126.

Bösenberg, J., 1998, "Ground-Based Differential Absorption Lidar for Water-Vapor and Temperature Profiling: Methodology," *Applied Optics*, Vol. 37, No. 18, pp. 3845-3860.

Brackley, I.J.A., 1971, "Partial Collapse in Unsaturated Expansive Clay," *Proc. 5th Regional Conference on Soil Mechanics and Foundation Engineering*, South Africa, pp. 23-30.

British Standard Institute (BSI), "Methods of Test for Soils for Civil Engineering Purposes." British Standard Institute, London, UK.

Bruneau, D., Quaglia, P., Flamant, C., Meissonnier, M., Pelon, J., 2001a, "Airborne Lidar LEANDRE II for Water-Vapor Profiling in the Troposphere. I. System Description" *Applied Optics*, Vol. 40, No. 21, pp. 3450-3461.

Bruneau, D., Quaglia, P., Flamant, C., Pelon, J., 2001b, "Airborne Lidar LEANDRE II for Water-Vapor Profiling in the Troposphere. II. First Results," *Applied Optics*, Vol. 40, No. 21, pp. 3462-3475.

Bufton, J.L., Itabe, T., Grolemund, D.A., 1983, "Airborne Remote Sensing Measurements with a Pulsed CO_2 Dial System," *Optical and Laser Remote Sensing*, Vol. 39, pp. 2-9.

Cannon, S.H. and Degraff J.V., 2009, "The Increasing Wildfire and Post-Fire Debris-Flow Threat in Western USA, and Implications for Consequences of Climate Change." *Landslides – Disaster Risk Reduction*, Vol. 177, No. 90. doi. 10.1007/978-3-540-69970-5_9.

Cannon, S.H. and Gartner, J.E., 2005, "Wildfire-related Debris Flow from a Hazards Perspective." In *Debris-flow Hazards and Related Phenomena* (pp. 363-385). Springer Berlin Heidelberg.

Cannon, S.H., Gartner, J.E., Rupert, M.G., Michael, J.A., Rea, A.H., Parrett, C., 2010, "Predicting the Probability and Volume of Post-Wildfire Debris Flows in the Intermountain West, USA." *Geological Society of America Bulletin*, Vol. 122, No. 1-2, pp. 127-144.

Cannon, S.H., Kirkham, R.M., Parise, M., 2000, "Wildfire-related Debris-flow Initiation Process, Storm King Mountain, Colorado." *Geomorphology*, Vol. 171, No. 88.

Carrier, W., Beckman, J., 1984, "Correlations between Index Properties of Remolded Clays." Geotechnique, Vol. 34, pp. 211-228.

Casagrande, A., 1958, "Notes on the Design of the Liquid Limit Device." Geotechnique, Vol. 8, No. 2, pp. 84-91.

Casagrande, A., Fadum, R., 1940, "Notes on Soil Testing for Engineering Purposes." Harvard Soil Mechanics, Series No. 8, Cambridge, Massachusetts.

Chabrillat, S., Goetz, A., Krosley, L., Olsen, H., 2002, "Use of Hyperspectral Images in the Identification and Mapping of Expansive Clay Soils and the Role of Spatial Resolution." Remote Sensing of Environment, Vol. 82, pp. 431-445.

Chang, C.W., Laird, D., Mausbach, M.J., Hurburgh, C.R., 2001, "Near-Infrared Reflectance Spectroscopy-Principle Components Regression Analysis of Soil Properties," *Soil Science Society of America Journal*, Vol. 65, pp. 480-490.

Clark, J., 2013, "Remote Sensing and Geospatial Support to Burned Area Emergency Response (BAER) Teams in Assessing Wildfire Effects to Hillslopes." In: Margottini C, Sassa K, Canuti P (eds) Landslide Science and Practice. Global Environmental Change, Springer, Heidelberg. pp 211-215.

Coffman, R.A., 2012, "Remote Sensing for Geotechnical Applications." National Academy of Sciences National Research Council Committee of Geological and Geotechnical Engineering Washington, D.C., November 15.

Collis, R.T.H., Russell, P.B., 1976, "Lidar Measurement of Particles and Gases by Elastic Backscattering and Differential Absorption," in *Laser Monitoring of the Atmosphere*. Ed. E.D. Hinkley. Springer-Verlag, New York.

Cozzolino, D., Moron, A., 2003, "The Potential of Near-Infrared Reflectance Spectroscopy to Analyze Soil Chemical and Physical Characteristics," *Journal of Agricultural Sciences*, Vol. 140, pp. 65-71.

Dalal, R., Henry, R., 1986, "Simultaneous Determination of Moisture, Organic Carbon, and Total Nitrogen by Near Infrared Reflectance Spectrophotometry," *Soil Science Society of America Journal*, Vol. 50, pp. 120-123.

De Graff, J.V., 2014, "Improvement in Quantifying Debris Flow Risk for Post-wildfire Emergency Response." *Geoenvironmental Disasters*. doi: 10.1186/s40677-014-0005-2.

De Graff, J.V., Lewis, D.S., 1989, "Using Past Landslide Activity to Guide Post-wildfire Mitigation." In: Watters RJ (ed) Engineering Geology and Geotechnical

Engineering, 25th Symposium on Engineering Geology and Geotechnical Engineering, Reno, NV, March 1989, Balkema, Rotterdam, pp. 65.
De Jong, S., 1993, "SIMPLS: An Alternative Approach to Partial Least Squares Regression", Chemometrics and Intelligent Laboratory Systems, 18:251-263.
Donovan, I.P. and Santi, P.M., 2017, "A Probabilistic Approach to Post-Wildfire Debris-Flow Volume Modeling." *Landslides*, Vol. 14, No. 4, pp.1345-1360.
Ehret, G., Kiemle, C., Renger, W., Simmet, G., 1993, "Airborne Remote Sensing of Tropospheric Water Vapor with a Near-Infrared Differential Absorption Lidar System," *Applied Optics*, Vol. 32, No. pp. 4534-4551.
Eaton, E.C., 1936, "Flood and Erosion Control Problems and Their Solution." ASCE Transactions, Vol. 101, No. 1, pp. 1302–1330.
Freedman, D.A., 1983, "A Note on Screening Regression Equations." *The American Statistician* 37.2: pp. 152-55.
Fredlund, D.G., 1981, "The Shear Strength of Unsaturated Soils and its Relationship to Slope Stability Problems in Hong Kong," *Hong Kong Engineer*, Hong Kong Institution of Engineers, April, pp. 37-45.
Garner, C.D., 2017, "Development of a Multiband Remote Sensing System for Determination of Unsaturated Soil Properties," Ph.D. Dissertation, University of Arkansas, Fayetteville, AR.
Gartner, J.E., Cannon, S.H., Bigio, E.R., Davis, N.K., Parrett, C., Pierce, K.L., Rupert, M.G., Thurston, B.L., Trebish, M.J., Garcia, S.P. and Rea, A.H., 2005, "Compilation of Data Relating To The Erosive Response of 608 Recently-Burned Basins in The Western United States (No. 2005-1218)."
Gartner, J.E., Cannon, S.H., Santi, P.M., deWolfe, V.G., 2008, "Empirical Models to Predict the Volumes of Debris Flows Generated by Recently Burned Basins in the Western U.S.," *Geomorphology*, Vol. 96, pp. 339-354.
Grant, W.B., 1982, "Effect of Differential Spectral Reflectance on DIAL Measurements Using Topographic Targets," *Applied Optics*, Vol. 21, No. 13, pp. 2390-2394.
Grant, W.B., 1991, "Differential Absorption and Raman Lidar for Water Vapor Profile Measurements: A Review," *Optical Engineering*, Vol. 30, No. 1, pp. 40-48.
Goetz, A., Chabrillat, S., and Lu, Z., 2001, "Field Reflectance Spectrometry for Detection of Swelling Clays at Construction Sites." Field Analytical Chemistry and Technology. Vol. 5, Issue 3, pp. 143-155.
Goetz, A., Olsen, H., Noe, D., Koehler, J., Humble, J., Fuschino, J., Johnson, E., Johnson, B., 2006, "Spectral Reflectance as a Rapid Technique for Field Determination of Soil Engineering Properties." Proceedings Geo-volution 2006, pp. 33-61.
Haigh, Stuart, 2012, "Mechanics of the Casagrande Limit Test." Canadian Geotechnical Journal, Vol. 49, No. 9, pp. 1015-1023.
Hammond, C.J., Prellwitz, R.W. and Miller, S.M., 1992, February. "Landslide Hazard Assessment Using Monte Carlo Simulation." In Proceedings of 6th international symposium on landslides, Christchurch, New Zealand, Balkema, Vol. 2, pp. 251-294.
Hapke, Bruce W., 2012, "*Theory of Reflectance and Emittance Spectroscopy." 2nd Edition*. Cambridge University Press, Cambridge, England.
Hardesty, R.M., 1984, "Coherent DIAL Measurement of Range-Resolved Water Vapor Concentration," *Applied Optics*, Vol. 23, No. 15, pp. 2545-2553.

Haupt SE, Pasini A, and Marzban C, eds., 2009,. *Artificial Intelligence Methods in the Environmental Sciences.* Springer.

Hey, J.V., Coupland, J., Foo, M.H., Richards, J., Sandford, A., 2011, "Determination of Overlap In Lidar Systems," *Applied Optics*, Vol. 50, No. 30, pp. 5791-5797.

Ho, D.Y.F., Fredlund, D.G., 1982, "Increase in Strength due to Suction for Two Hong Kong Soils," *Proc. ASCE Conference on Engineering and Construction in Tropical and Residual Soils*, Honolulu, USA, pp. 263-295.

Hsieh, W.W., 2009, "Machine Learning Methods in the Environmental Sciences." *Neural Networks and Kernels*. UK Cambridge UP. doi: 10.1017/CBO9780511627217.

Hungr, O., Morgan, G.C. and Kellerhals, R., 1984, "Quantitative Analysis of Debris Torrent Hazards for Design of Remedial Measures." *Canadian Geotechnical Journal*, Vol. 21, No. 4, pp. 663-677.

Ishii, S., Koyama, M., Baron, P., Iwai, H., Mizutani, K., Itabe, T., Sato, A., Asai, K., 2013, "Ground-Based Integrated Path Coherent Differential Absorption Lidar Measurement of CO_2: Foothill Target Return," Amtospheric Measurement Techniques, Vol. 6, pp. 1359-1369.

Ismail, S., Browell, E.V., 1989, "Airborne and Spaceborne Lidar Measurements of Water Vapor Profiles: A Sensitivity Analysis," *Applied Optics*, Vol. 28, No. 23, pp. 3603-3614.

Islam, K., Singh, B., McBratney, A., 2003, "Simultaneous Estimation of Various Soil Properties By Ultra-Violet, Visible, and Near-Infrared Reflectance Spectroscopy," *Australian Journal of Soil Research*, Vol. 41, pp. 1101-1114.

Janik, L., Skjemstad, J., Raven, M., 1995, "Characterization and Analysis of Soils Using Mid-Infrared Partial Least-Squares. I. Correlations with XRF-Determined Major-Element Compositions," *Australian Journal of Soil Research*, Vol. 33, pp. 621-636.

Janik, L., Skjemstad, J., 1995, "Characterization and Analysis of Soils Using Mid-Infrared Partial Least Squares: II. Correlations with Some Laboratory Data," *Australian Journal of Soil Research*, Vol. 33, pp. 637-650.

Jelalian, A. 1992. "*Laser Radar Systems*." Artech House, Massachusetts.

Jenkins, F.A., and White, H.E. 1937. "*Fundamentals of Physical Optics*." McGraw-Hill, New York.

Johnson, P.A., McCuen, R.H. and Hromadka, T.V., 1991, "Magnitude and Frequency of Debris Flows." *Journal of Hydrology*, Vol. 123, No. 1-2, pp. 69-82.

Karlsson, C.J. Olsson, F.Å.A., 1999, "Linearization of the Frequency Sweep of a Frequency-Modulated Continuous-Wave Semiconductor Laser and the Resulting Ranging Performance," *Applied Optics*, Vol. 38, No. 15, pp. 3376-3386.

Kern, A.N., Addison, P., Oommen, T., Salazar, S.E., Coffman, R.A., 2017, "Machine Learning Based Predictive Modeling of Debris Flow Probability Following Wildfire in the Intermountain Western United States," *Mathematical Geosciences*, doi: 10.1007/s11004-017-9681-2.

Krahn, J., Fredlund, D.G., Klassen, M.J., 1989, "Effect of Soil Suction on Slope Stability at Notch Hill," *Canadian Geotechnical Journal*, Vol. 26, pp. 269-278.

Krasnopolsky, V.M., 2007, "Neural Network Emulations for Complex Multidimensional Geophysical Mappings: Applications of Neural Network Techniques to

Atmospheric and Oceanic Satellite Retrievals and Numerical Modeling." *Reviews of Geophysics,* Vol. 45, No. 3, RG3009, doi:10.1029/2006RG000200.
Kodaira, M., Shibusawa, S., 2013, "Using a Mobile Real-Time Soil Visible Infrared Sensor for High Resolution Soil Properties Mapping." *Geoderma*, Vol. 199, pp. 64-79.
Kou, L. D. Labfie, and P. Chylek, 1993, "Refractive Indices of Water and Ice in the 0.65- to 2.5-mm Spectra Range." Appl.Opt., Vol. 32, 3531-3540.
Kubelka, P., Munk, F., 1931, "Ein Beitrag zur Optik der Farbanstriche," *Zeitschrift für Technische Physik*, Vol. 12, pp. 593-601 (in German).
Kubelka, P., 1948, "New Contributions to the Optics of Intensely Light-Scattering Materials. Part I," *Journal of the Optical Society of America*, Vol. 38, No. 5, pp. 448-457.
Kuhn, M., and Johnson, K., 2013, "Applied Predictive Modeling." New York, NY: Springer.
Kulhawy, F., Mayne P., 1990, "Manual on Estimating Soil Properties for Foundation Design." Final Report of the Electric Power Research Institute Research Project 1493-6.
Little, L.M., Papen, G.C., 2001, "Fiber-Based Lidar for Atmospheric Water-Vapor Measurements," *Applied Optics*, Vol. 40, No. 21, pp. 3417-3427.
Lumb, P., 1975, "Slope Failures in Hong Kong," *Quarterly Journal of Engineering Geology*, Vol. 8, pp. 31-65.
Mathworks, 2014, "The MATLAB R2014A Programming Suite and Supporting Documentation" The Mathworks Corporation, Natick, Massachusetts.
Mathworks, 2010, "Plsregress.m" Partial Least Squares Regression Software. The Mathworks Corporation, Natick, Massachusetts.
Mathworks, 2012, "Pca.m" Principle Components Analysis Software. The Mathworks Corporation, Natick, Massachusetts.
Machol, J.L., Ayers, T., Schwenz, K.T., Koenig, K.W., Hardesty, R.M., Senff, C.J., Krainak, M.A., Abshire, J.B., Bravo, H.E., Sandberg, S.P., 2004, "Preliminary Measurements with an Automated Compact Differential Absorption Lidar for the Profiling of Water Vapor," *Applied Optics*, Vol. 43, No. 15, pp. 3110-3121.
Maiman, T.H., 1960, "Stimulated Optical Radiation in Ruby," *Nature*, Vol. 187, pp. 493-494.
McCarty, G., Reeves, J., Reeves, V., Follet, R., Kimble, J., 2002, "Mid-Infrared and Near-Infrared Diffuse Reflectance Spectroscopy for Soil Carbon Measurement." *Soil Science Society of America Journal*, Vol. 66, pp. 640-646.
McClung, F.J., Hellarth, R.W., 1962, "Giant Optical Pulsations from Ruby," *Journal of Applied Physics*, Vol. 33, pp. 828-829.
Megie, G., Menzies, R.T., 1980, "Complementarity of UV and IR Differential Absorption Lidar for Global Measurements of Atmospheric Species," *Applied Optics*, Vol. 19, No. 7, pp. 1173-1183.
Menzies, R.T., Shumate, M.S., 1976, "Remote Measurements of Ambient Air Pollutants with a Bistatic Laser System," *Applied Optics*, Vol. 15, No. 9, pp. 2080-2084.
Middleton, W.E.K., Spilhaus, A.F., 1953, "*Meteorological Instruments."* University of Toronto Press, Toronto, Canada,

Morris, P., Lockington, D., Apelt, C., 2000, "Correlations for Mine Tailings Consolidation Parameters." International Journal of Surface Mining, Reclamation and Environment, Vol. 14, pp. 171-443.
Negri, J.A., 2016, "Evaluation and Validation of Multiple Predictive Models Applied to Post-Wildfire Debris-Flow Hazards," M.S. thesis, Colorado School of Mines, Golden, CO.
Nehrir, A.R., 2008, "Water Vapor Profiling Using a Compact Widely Tunable Diode Laser Differential Absorption Lidar (DIAL)," M.S. thesis, Montana State University, Bozeman, MT.
Nehrir, A.R., 2011, "Development of an Eye-Safe Diode-Laser-Based Micro-Pulse Differential Absorption Lidar (MP-DIAL) for Atmospheric Water-Vapor and Aerosol Studies," Ph.D. Dissertation, Montana State University, Bozeman, MT.
Nehrir, A.R., Repasky, K.S., Carlsten, J.L., Obland, M.D., Shaw, J.A., 2009, "Water Vapor Profiling Using a Widely Tunable, Amplified Diode-Laser-Based Differential Absorption Lidar (DIAL)," *Journal of Atmospheric and Oceanic Technology*, Vol. 26, No. 4, pp. 733-745.
Nehrir, A.R., Repasky, K.S., Carlsten, J.L., 2011, "Eye-Safe Diode-Laser-Based Micropulse Differential Absorption Lidar (DIAL) for Water Vapor Profiling in the Lower Troposphere," *Journal of Atmospheric and Oceanic Technology*, Vol. pp. 131-147.
Nehrir, A.R., Repasky, K.S., Carlsten, J.L., 2012, "Micropulse Water Vapor Differential Absorption Lidar: Transmitter Design and Performance," *Optics Express*, Vol. 20, No. 22, pp. 25137-25151.
Nicolet, 2004, "Nicolet FT-IR User's Guide." Nicolet 6700 Fourier Transform Infrared Spectrometer User's Manual and Supporting Documentation.
Nocita, M., Stevens, A., Noon, C., van Wesemael., 2013, "Predication of Soil Organic Carbon for Different Levels of Soil Moisture Using Vis-NIR Spectroscopy." Geoderma, Vol. 199, pp. 37-42.
NASA, 2011, "Earth Observatory." National Aeronautic and Space Administration, Washington, http://earthobservatory.nasa.gov/GlobalMaps/view.php.
NIFC, 2017, "Fire Info." https://www.nifc.gov/fireInfo/nfn.htm.
Olden, J.D., and Jackson, D.A., 2002, "A Comparison of Statistical Approaches for Modeling Fish Species Distributions." *Freshwater Biology*, Vol. 47, No. 10, pp. 1976-95
Oppenheim, U.P., Menzies, R.T., 1982, "Aligning the Transmitter and Receiver Telescopes of an Infrared Lidar: A Novel Method," *Applied Optics*, Vol. 21, No. 2, pp. 174-175.
Park, J.K., 1980, "A Soil Moisture Reflectance Model in Visible and Near IR Bands," *Proc. Symposium on Machine Processing of Remotely Sensed Data and Soil Information Systems and Remote Sensing and Soil Survey*, Purdue University, West Lafayette, USA.
Pierrottet, D., Amzajerdian, F., Peri, F., 2005, "Development of an All-Fiber Coherent LaserRadar for Precision Range and Velocity Measurements," *Proc. Materials Research Society Symposium*, Vol. 833,
Pierrottet, D., Amzajerdian, F., Petway, L., Barnes, B., Lockard, G., Rubio, M., 2008, "Linear FMCW Laser Radar for Precision Range and Vector Velocity

Measurements," *Proc. Materials Research Society Symposium*, Vol. 1076, San Francisco, USA.
Philpot, W.D., Tian, J., 2016, "The Hyperspectral Soil Line: A Preliminary Description," *Light, Energy, and the Environment*, OSA Technical Digest (Online), Optical Society of America, paper HW3E.2, 3 pgs.
Pope, R.M, Fry, E.S., 1997, "Absorption Spectrum (380-700 nm) of Pure Water. II. Integrating Cavity Measurements." Appl. Opt. Vol. 36, 8710-8723.
Prasad, N.S., Geiger, A.R., 1996, "Remote Sensing of Propane and Methane by Means of a Differential Absorption Lidar by Topographic Reflection," *Optical Engineering*, Vol. 35, No. 4, pp. 1105-1111.
Remsberg, E.E., and Gordley, L.L., 1978, "Analysis of Differential Absorption Lidar from the Space Shuttle." Vol. 17, No. 4, pp.624-630.
Repasky, K.S., 2016. Personal correspondence. July 19, 2016.
Repasky, K.S., Moen, D., Spuler, S., Nehrir, A.R., Carlsten, J.L., 2013, "Progress towards an Autonomous Field Deployable Diode-Laser-Based Differential Absorption (DIAL) for Profiling Water Vapor in the Lower Troposphere," *Remote Sensing*, Vol. 5, No. 12, pp. 6241-6259.
Rosipal, R. and Kramer, N., 2006, "Overview and Recent Advances in Partial Least Squares", in Subspace, Latent Structure and Feature Selection: Statistical and Optimization Perspectives Workshop (SLSFS 2005), Revised Selected Papers (Lecture Notes in Computer Science 3940), C.Saunders et al. (Eds.) pp. 34-51, Springer.
Rossel, R., McBratney, A., Minasny, B. (eds.), 2010, "Proximal Soil Sensing. Volume 1 of Progress in Soil Science." Springer Science and Business Media.
Rothman, L.S., Gordon, I.E., Babikov, Y., Barbe, A., Chris Benner, D., Bernath, P.F., Birk., M., Bizzocchi, L., Boudon, V., Brown, L.R., Campargue, A., Chance, K., Cohen, E.A., Coudert, L.H., Devi, V.M., Drouin, B.J., Fayt, A., Flaud, J.-M., Gamache, R.R., Harrison, J.J., Hartmann, J.-M., Hill, C., Hodges, J.T., Jacquemart, D., Jolly, A., Lamouroux, J., Le Roy, R.J., Li, G., Long, D.A., Lyulin, O.M., Mackie, C.J., Massie, S.T., Mikhailenko, S., Müller, H.S.P., Naumenko, O.V., Nikitin, A.V., Orphal, J., Perevalov, V., Perrin, A., Polovtseva, E.R., Richard, C., Smith, M.A.H., Starikova, E., Sung, K., Tashkun, S., Tennyson, J., Toon, G.C., Tyuterev, VI.G., Wagner, G., 2013, "The HITRAN2012 Molecular Spectroscopic Database," *Journal of Quantitative Spectroscopy and Radiative Transfer*, Vol. 130, pp. 4-50.
Samui, P., Gowda, P., Oommen, T., Howell, T., Marek, T., 2012, "Statistical Learning Algorithms for Identifying Contrasting Tillage Practices with Landsat Thematic Mapper Data." *International Journal of Remote Sensing.* pp. 5732-5745.
Santi, P.M., Victor, G., Dewolfe, J.V., Higgins, D., Cannon, S.H., and Gartner, J.E., 2007, "Sources of Debris Flow Material in Burned Areas." *Geomorphology*: 310-21
Schotland, R.M., 1966, "Some Observations of the Vertical Profile of Water Vapor by a Laser Optical Radar," *Proc. Fourth Symposium on Remote Sensing of the Environment*, Ann Arbor, USA, pp. 273-283.
Schotland, R.M., 1974, "Errors in the Lidar Measurement of Atmospheric Gases by Differential Absorption," *Journal of Applied Meteorology*, Vol. 13, pp. 71-77.

Shepherd, K.D., Walsh, M.G., 2002, "Development of Reflectance Spectral Libraries for Characterization of Soil Properties," *Soil Science Society of America Journal*, Vol. 66, pp. 988-998.

Shibusawa, S., Imade-Amon, S., Sato, S., Sasao, A., Harako, S., 2001, "Soil Mapping Using the Real-Time Soil Spectrophotometer." Proceedings of the Third European Conference on Precision Agriculture, Vol. 1, Agro Montpellier, pp. 497-508.

Skempton, A., 1944, "Notes on the Compressibility of Clays." Quarterly Journal of the Geological Society of London, Vol. 100, C: Parts 1 and 2. Pp. 119-135.

Skempton, A., Northey, R., 1953, "The Sensitivity of Clays." Geotechnique, Vol. 3, No. 1, pp. 30-53.

Skolnik, M.I., 1960, "Theoretical Accuracy of Radar Measurements," *IRE Transactions on Aeronautical and Navigational Electronics*, pp. 123-129.

Spuler, S.M., Repasky, K.S., Morley, B., Moen, D., Hayman, M., Nehrir, A.R., 2015, "Field-Deployable Diode-Laser-Based Differential Absorption Lidar (DIAL) for Profiling Water Vapor," *Atmospheric Measurement Techniques*, Vol. 8, pp. 1073-1087.

Spuler, S., Repasky, K., Morley, B., Moen, D., Weckwerth, T., Hayman, M., Nehrir, A., 2016, "Advances in Diode-Laser-Based Water Vapor Differential Absorption Lidar," *Proc. International Laser Radar Conference*, July 2015, New York City, USA.

Staley, D.M., Kean, J.W., Cannon, S.H., Schmidt, K.M. and Laber, J.L., 2013, "Objective Definition Of Rainfall Intensity–Duration Thresholds For The Initiation Of Post-Fire Debris Flows In Southern California." *Landslides*, Vol. 10, No. 5, pp. 547-562.

Staley, D.M., Negri, J.A., Kean, J.W., Laber, J.L., Tillery, A.C. and Youberg, A.M., 2016, "Updated Logistic Regression Equations For The Calculation of Post-Fire Debris-Flow Likelihood in the Western United States (No. 2016-1106)." US Geological Survey.

Staley, D.M., Negri, J.A., Kean, J.W., Laber, J.L., Tillery, A.C. and Youberg, A.M., 2017, "Prediction of Spatially Explicit Rainfall Intensity–Duration Thresholds For Post-Fire Debris-Flow Generation in the Western United States." *Geomorphology*, Vol. 278, pp.149-162.

Steyerberg, E.W., and Harrell, F.E., 2015, "Prediction Models Need Appropriate Internal, Internal–external, and External Validation." Journal of Clinical Epidemiology.

Stenberg, B., Viscarra Rossel, R.A., "Diffuse Reflectance Spectroscopy for High-Resolution Soil Sensing," in *Proximal Soil Sensing. Volume 1 of Progress in Soil Science*. Eds. R.A. Viscarra Rossel, A.B. McBratney, B. Minasny. Springer Science+Business Media, New York, 2010.

Taylor, D.D., 1948, "Fundamentals of Soil Mechanics." John Wiley and Sons, Inc., New York.

Terzhagi, K., Peck, R., Mesri, G., 1996, "Soil Mechanics in Engineering Practice," 3 ed., John Wiley and Sons, Hoboken, NJ.

Tian, J., Philpot, W.D., 2015, Relationship Between Surface Soil Water Content, Evaporation Rate, and Water Absorption Band Depths in SWIR Reflectance Spectra," *Remote Sensing of Environment*, Vol. 169, No. pp. 280-289.

Wallace, A.M, Gibson, G., Lamb, R.A., 2005, "Multi-spectral Laser Detection and Ranging for Range Profiling and Surface Characterization," *Journal of Optics A: Pure and Applied Optics*, Vol. 7, pp. S438-S444.

Walvoort, A., McBratney, A., 2001, "Diffuse Reflectance Spectrometry as a Proximal Sensing Tool for Precision Agriculture," *Proc. 3rd European Conference on Precision Agriculture*, Agro Montpellier, France, pp. 503-508.

Wandinger, Ulla, 2005, "Introduction to Lidar," in *Lidar: Range-Resolved Optical Remote Sensing ofThe Atmosphere*. Ed. Claus Weitkamp. Springer Science+Business Media, New York.

Waruru, B., Shepard, K., Ndegwa, G., Kamoni, P., Sila, A., 2014, "Rapid Estimation of Soil Engineering Properties Using Diffuse Reflectance Near Infrared Spectroscopy." Journal of Biosystems Engineering, Vol. 121, pp. 177-185.

Weckwerth, T.M., Weber, K.J., Turner, D.D., Spuler, S.M., 2016, "Validation of a Water Vapor Micropulse Differential Absorption Lidar (DIAL)," *Journal of Atmospheric and Oceanic Technology*, Vol. 33, No. 11, pp. 2353-2372.

Weitkamp, Claus, 2005, "Lidar: Introduction," in *Laser Remote Sensing*. Eds. Takashi Fujii, TetsuoFukuchi. Taylor & Francis Group, Florida, pp. 2-36.

Wells, W.G. II, 1987, "The Effects of Fire on the Generation of Debris Flows in Southern California." Geological Society of America Reviews in Engineering Geology, 7, pp. 105–114.

Whiting, M.L., Li, L., Ustin, S.L., 2004, "Predicting Water Content Using Gaussian Model on Soil Spectra," *Remote Sensing of Environment*, Vol. 89, No. 4, pp. 535-552.

Wold, S., Sjostrom, M., Eriksson, L., 2001, "PLS-Regression: A Basic Tool of Chemometrics." Chemometrics and Intelligent Laboratory Systems. Vol. 58, Issue 2, pp. 109-130.

Wroth, C., Wood, D., 1978, "The Correlation of Index Properties with Some Basic Engineering Properties of Soils." Canadian Geotechnical Journal, Vol. 15, No. 2, pp. 137-145.

Wulf, H., Mulder, T., Schaepman, M.E., Keller, A., Jörg, P.C., 2015, "Remote Sensing of Soils," Report prepared by Remote Sensing Laboratories, Dept. of Geography, University of Zurich, Switzerland, 71 pgs.

Wulfmeyer, V., 1998, "Ground-Based Differential Absorption Lidar for Water-Vapor and Temperature Profiling: Development and Specifications of a High-Performance Laser Transmitter," *Applied Optics*, Vol. 37, No. 18, pp. 3804-3824.

Wulfmeyer, V., Bösenberg, J., 1998, "Ground-Based Differential Absorption Lidar for Water-Vapor Profiling: Assessment of Accuracy, Resolution, and Meteorological Applications," *Applied Optics*, Vol. 37, No. 18, pp. 3825-3844.

Wulfmeyer, V., Walther, C., 2001, "Future Performance of Ground-Based and Airborne Water-Vapor Differential Absorption Lidar. I. Overview and Theory," *Applied Optics*, Vol. 40, No. 30, pp. 5304-5320.

Yitagesu, F., van der Meer, F., van der Werff, H., Zigterman, W., 2009, "Quantifying Engineering Parameters of Expansive Soils from Their Reflectance Spectra." *Engineering Geology*, Vol. 105, Issue 3-4, pp. 151-160.

Youssef, M., El Ramli, A., El Demery, M., 1965, "Relationships between Shear Strength, Consolidation, Liquid Limit, and Plastic Limit for Remoulded Clays."

Proceedings of the 6th International Conference on Soil Mechanics and Foundation Engineering, Montreal, Vol. 1, pp. 126-129.